AD-A034 325 KAMAN AVIDYNE BURLINGTON MASS F/G 9/5
FINITE ELEMENT ANALYSIS OF THE BLAST RESPONSE OF A COMPLETE SHE--ETC(U)
DEC 76 J M CALLIGEROS, J P WALSH DAAD05-74-C-0744
UNCLASSIFIED KA-TR-122 BRL-CR-324 NL

1 OF 1
AD-A
034 325

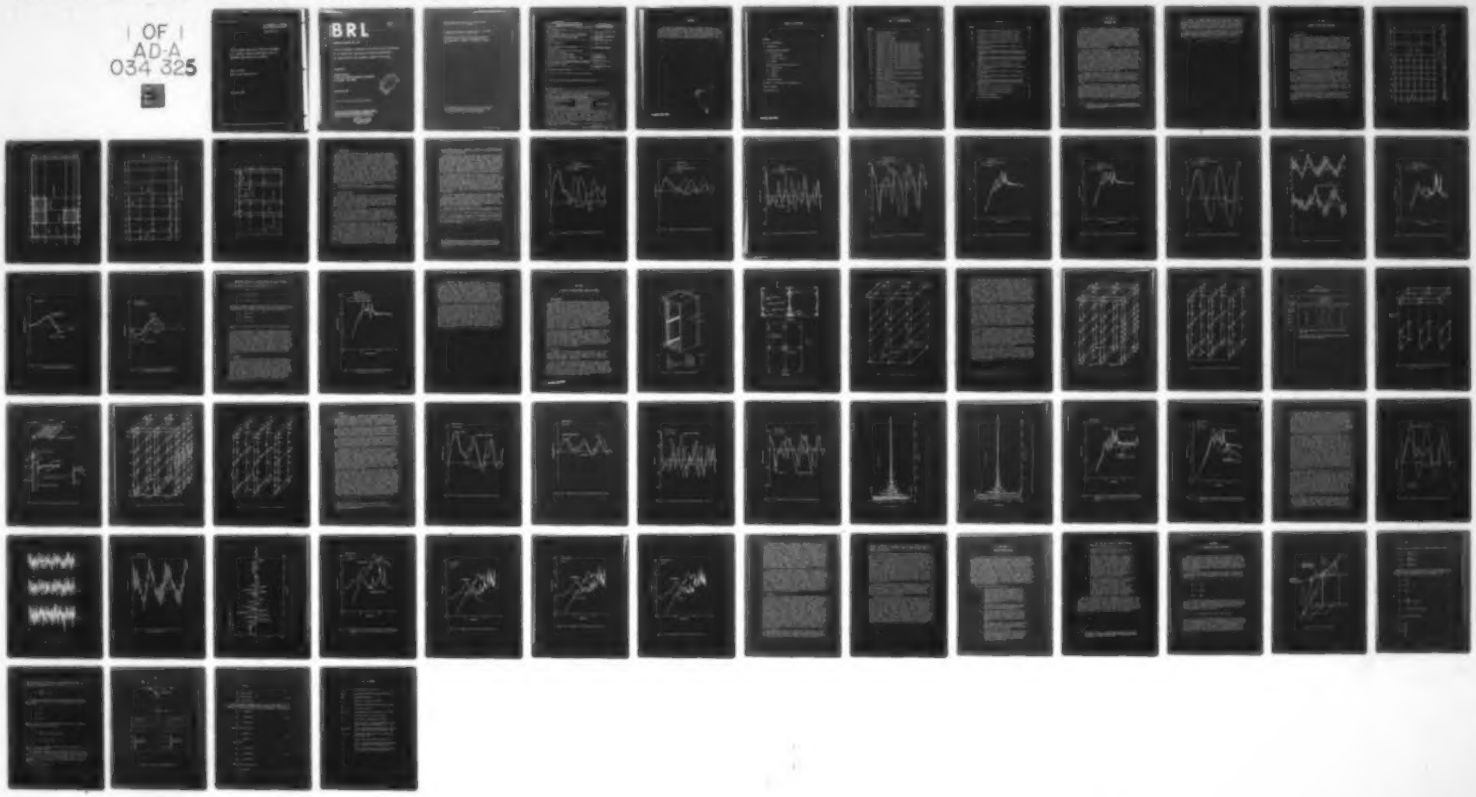

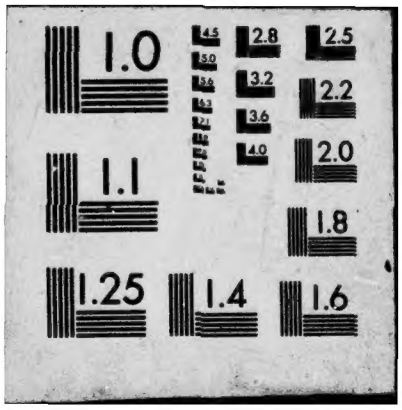
1.0
1.1
1.25
1.4
1.6
1.8
2.0
2.2
2.5
2.8
3.2
3.6
4.0
4.5
5.0
5.6

FINITE ELEMENT ANALYSIS OF THE BLAST RESPONSE OF A COMPLETE SHELTER SYSTEM AND EFFECTS OF EQUIPMENT RACK MODEL MODIFICATIONS

KAMAN AVIDYNE
BURLINGTON, MASSACHUSETTS

DECEMBER 1976

BRL CR 324

BRL

AD

CONTRACT REPORT NO. 324

FINITE ELEMENT ANALYSIS OF THE BLAST RESPONSE OF A COMPLETE SHELTER SYSTEM AND EFFECTS OF EQUIPMENT RACK MODEL MODIFICATIONS

Prepared by

Kaman AviDyne
A Division of Kaman Sciences Corporation
Burlington, MA 01803

December 1976

USA BALLISTIC RESEARCH LABORATORIES
ABERDEEN PROVING GROUND, MARYLAND

Destroy this report when it is no longer needed.
Do not return it to the originator.

Secondary distribution of this report by originating or sponsoring activity is prohibited.

Additional copies of this report may be obtained from the National Technical Information Service, U.S. Department of Commerce, Springfield, Virginia 22151.

The findings in this report are not to be construed as an official Department of the Army position, unless so designated by other authorized documents.

UNCLASSIFIED

SECURITY CLASSIFICATION OF THIS PAGE *(When Data Entered)*

REPORT DOCUMENTATION PAGE		READ INSTRUCTIONS BEFORE COMPLETING FORM
1. REPORT NUMBER BRL CONTRACT REPORT NO. 324	2. GOVT ACCESSION NO.	3. RECIPIENT'S CATALOG NUMBER
4. TITLE *(and Subtitle)* FINITE ELEMENT ANALYSIS OF THE BLAST RESPONSE OF A COMPLETE SHELTER SYSTEM AND EFFECTS OF EQUIPMENT RACK MODEL MODIFICATIONS		5. TYPE OF REPORT & PERIOD COVERED Final Report 1 Nov 1972 - 30 Jun 1975 6. PERFORMING ORG. REPORT NUMBER KA TR-122
7. AUTHOR(s) John M. Calligeros John P. Walsh		8. CONTRACT OR GRANT NUMBER(s) DAAD05-74-C-0744
9. PERFORMING ORGANIZATION NAME AND ADDRESS Kaman AviDyne A Division of Kaman Sciences Corporation Burlington, MA 01803		10. PROGRAM ELEMENT, PROJECT, TASK AREA & WORK UNIT NUMBERS
11. CONTROLLING OFFICE NAME AND ADDRESS USA Ballistic Research Laboratory Aberdeen Proving Ground, Maryland 21005		12. REPORT DATE DECEMBER 1976 13. NUMBER OF PAGES ~~86~~ 74
14. MONITORING AGENCY NAME & ADDRESS *(if different from Controlling Office)* US Army Materiel Development & Readiness Command 5001 Eisenhower Avenue Alexandria, VA 22333		15. SECURITY CLASS. *(of this report)* UNCLASSIFIED 15a. DECLASSIFICATION/DOWNGRADING SCHEDULE

16. DISTRIBUTION STATEMENT *(of this Report)*

Approved for public release; distribution unlimited.

17. DISTRIBUTION STATEMENT *(of the abstract entered in Block 20, if different from Report)*

18. SUPPLEMENTARY NOTES

This research was sponsored by the Defense Nuclear Agency under Subtask V99QAXNB005, Work Unit Code 05, Military Equipment Vulnerability; and Army Project DA No. 1W162118AH75, AMCMS Code 632306.11.H7200, Nuclear Weapons Effects for Army Applications, Blast and Shock.

19. KEY WORDS *(Continue on reverse side if necessary and identify by block number)*

Finite Element Modeling	Shock Spectra Correlation	
Electronic Equipment Shelters	Structural Response	
Blast Response	Shock and Vibration	Structural Dynamics
DIAL PACK	Guy Cable Modeling	Blast Loading
Acceleration Correlation	NASTRAN Modeling	

20. ABSTRACT *(Continue on reverse side if necessary and identify by block number)*

The transient blast response of an Army S-280 shelter containing electronic equipment racks was obtained with the NASTRAN finite element code. Results using a model of the complete shelter-rack system in a tie-down condition are compared with results obtained with a simpler model consisting of the front wall and front racks. Modifications are made to the finite element model of the rack. Comparisons are made between the NASTRAN responses and data obtained from the DIAL PACK field test for accelerations and shock spectra on the front wall and front rack.

DD FORM 1 JAN 73 1473 EDITION OF 1 NOV 65 IS OBSOLETE

UNCLASSIFIED

SECURITY CLASSIFICATION OF THIS PAGE *(When Data Entered)*

FOREWORD

This work was performed for Ballistic Research Laboratories under Contract Number DAAD05-74-C-0744 by Kaman AviDyne, Burlington, Mass., a division of Kaman Sciences Corporation. The technical monitor for BRL was Dr. W. Don Allison. Mr. John M. Calligeros was the project leader and principal investigator of the study which was performed in the Structural Mechanics Group of Kaman AviDyne headed by Mr. E.S. Criscione.

Preceding page blank

TABLE OF CONTENTS

LIST OF ILLUSTRATIONS

LIST OF ILLUSTRATIONS (Concluded)

SECTION 1

INTRODUCTION

This report is a continuation and extension of the analysis initiated in Ref. 1 of the response of electrical equipment shelters and of the associated internally mounted electronic equipment to blast loading. The accelerations experienced by the rack-mounted equipment may result in malfunctioning or complete disablement of the equipment and thus a need exists for suitable analytical methods of analysis. The problem is inherently complex since the equipment is mounted on racks whose structural response is dependent not only on the rack structure and mounting arrangement but also on the response of a flexible shelter engulfed by a time varying blast load. The shelter response in turn is also coupled to the rack response.

The finite element method of analysis is particularly attractive for analyzing this problem because of the complex structural configuration involved. In Ref. 1 the NASTRAN code was used for this purpose and a model of a complete Army S-280 shelter in a tie-down condition containing commercially available equipment racks was assembled for NASTRAN. Computer runs using a simplified model consisting of the front wall and front racks were made for a blast loading corresponding to the DIAL PACK field test. Comparisons were made with the test data and the results showed that generally the front wall accelerations were consistent with the test measurements but that the analytical rack accelerations were considerably lower than the test results. NASTRAN runs of the complete shelter system were not available at that time.

The present report has two primary objectives. The first is to present NASTRAN responses on the front wall and rack using the complete shelter model and to compare with the responses obtained with the simpler model of Ref. 1. In conjunction with this, a more general model of the cable forces is presented and the influence of the cables is assessed.

The second objective of the report is to refine the original finite element model of the rack for the purpose of improving the comparison of the analytically obtained rack accelerations with the test data. The rack model modifications include a better definition of the load path within the rack, the introduction of additional grid points and structural elements and the inclusion of the stiffening effects of the rack shelves which were previously neglected (originally, only the shelf mass was modeled). The original rack model, having less structural detail, in

---

Ref. 1. Calligeros, J.M. and Walsh, J.P., Finite Element Modeling of Army Electronic Equipment Shelters Subjected to Blast Loading, KA TR-109, July 1974.

essence "filters" out high frequency components which could affect the total response. The modifications made to the rack model introduce additional degrees-of-freedom which represent these higher harmonics. Responses are obtained for three rack modifications of increasing complexity and comparisons are made with the responses obtained with the original less detailed rack model of Ref. 1 and with the test data.

Section 2 of the report compares NASTRAN responses obtained with the complete shelter model and with the simpler model. The rack modeling modifications and comparisons with the test data are given in Section 3. The major conclusions are summarized in Section 4.

SECTION 2

COMPLETE SHELTER RESPONSE

2.1 Introduction

In Ref. 1, time history responses and acceleration shock spectra were obtained at selected structural locations on the front wall and front racks of an S-280 shelter subjected to a blast load. These calculations were determined for a simplified model of the shelter consisting only of the front wall and front racks using the finite element code NASTRAN. A complete structural and loading model of the shelter was also developed in Ref. 1 but NASTRAN responses were not available for publication at that time.

This section of the report presents time history responses and shock spectra for the same structural locations of Ref. 1, but using the complete NASTRAN structural model of the shelter in a tie-down condition. The finite element model of the shelter structure as well as the loading models for the front, rear and end walls and the roof, are described in detail in Ref. 1 and will not be repeated here. A more general model of the tie-down cables than the one presented in Ref. 1, which also includes the effect of a tensile preload, was subsequently developed and is described herein in Appendix A.

The grid system of the shelter walls and roof is shown in Figs. 2.1 - 2.4 and the grid system of the front racks is shown in Fig. 3.3 of Section 3. Due to existing structural and loading symmetries with respect to a centerplane perpendicular to the front wall, it was necessary to model only half of the shelter-rack system. As a result, 176 degrees-of-freedom were used to describe the dynamic response of the complete system, assuming the shelter floor is clamped to the ground.

The loading consists of a shock wave impinging on the front wall (side-on) and engulfing the complete shelter at a finite rate. The strength of the shock is 2.61 psi incident overpressure, corresponding to the DIAL PACK event discussed in Ref. 1.

NASTRAN responses were obtained with this complete shelter model and were compared with the results of the simpler model of Ref. 1, assessing also the influence of the tie-down cables. The direct transient solution technique in NASTRAN was used to obtain the dynamic responses.

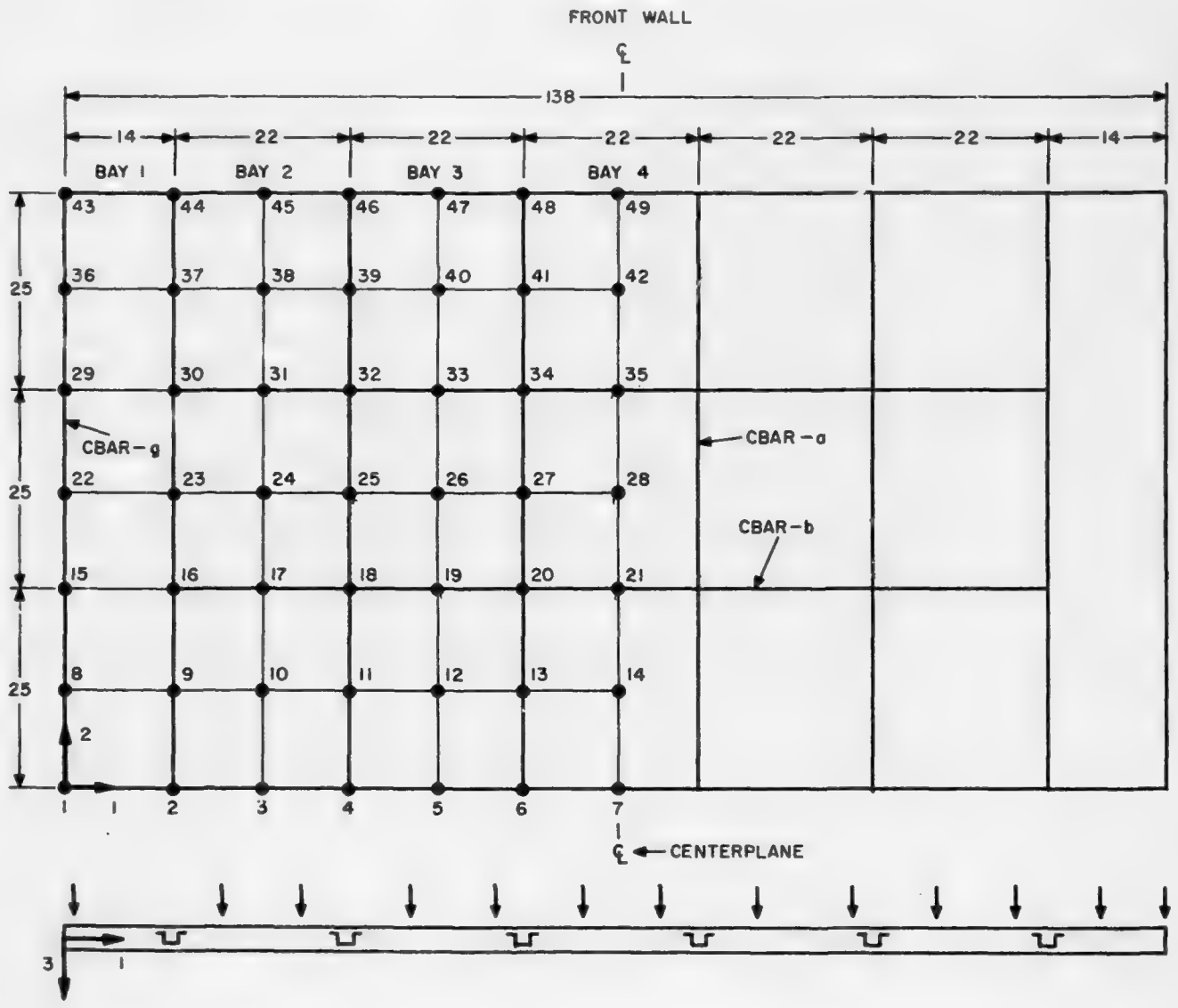

Figure 2.1 - Front Wall Grid System

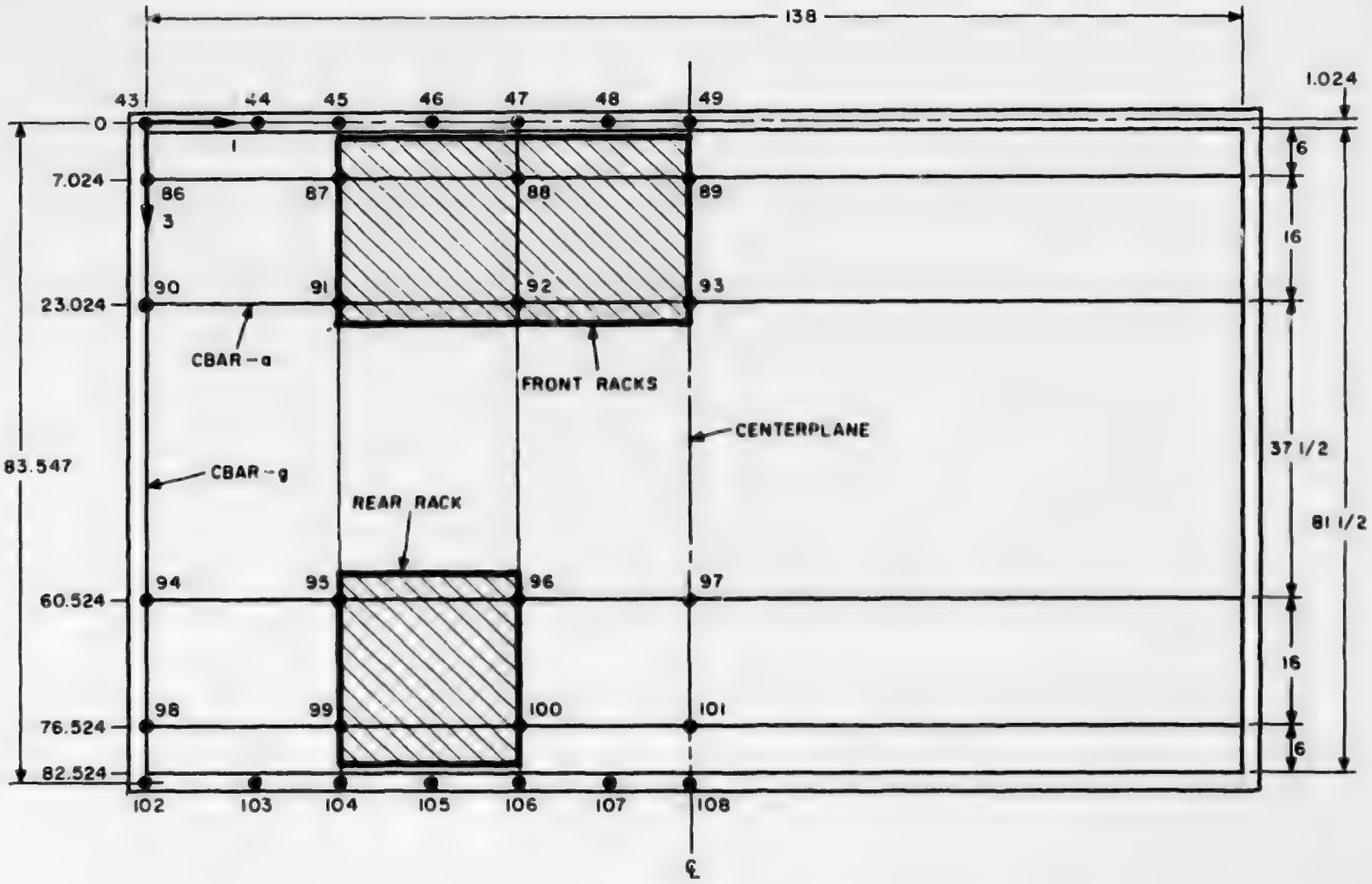

Figure 2.2 - Roof Grid System

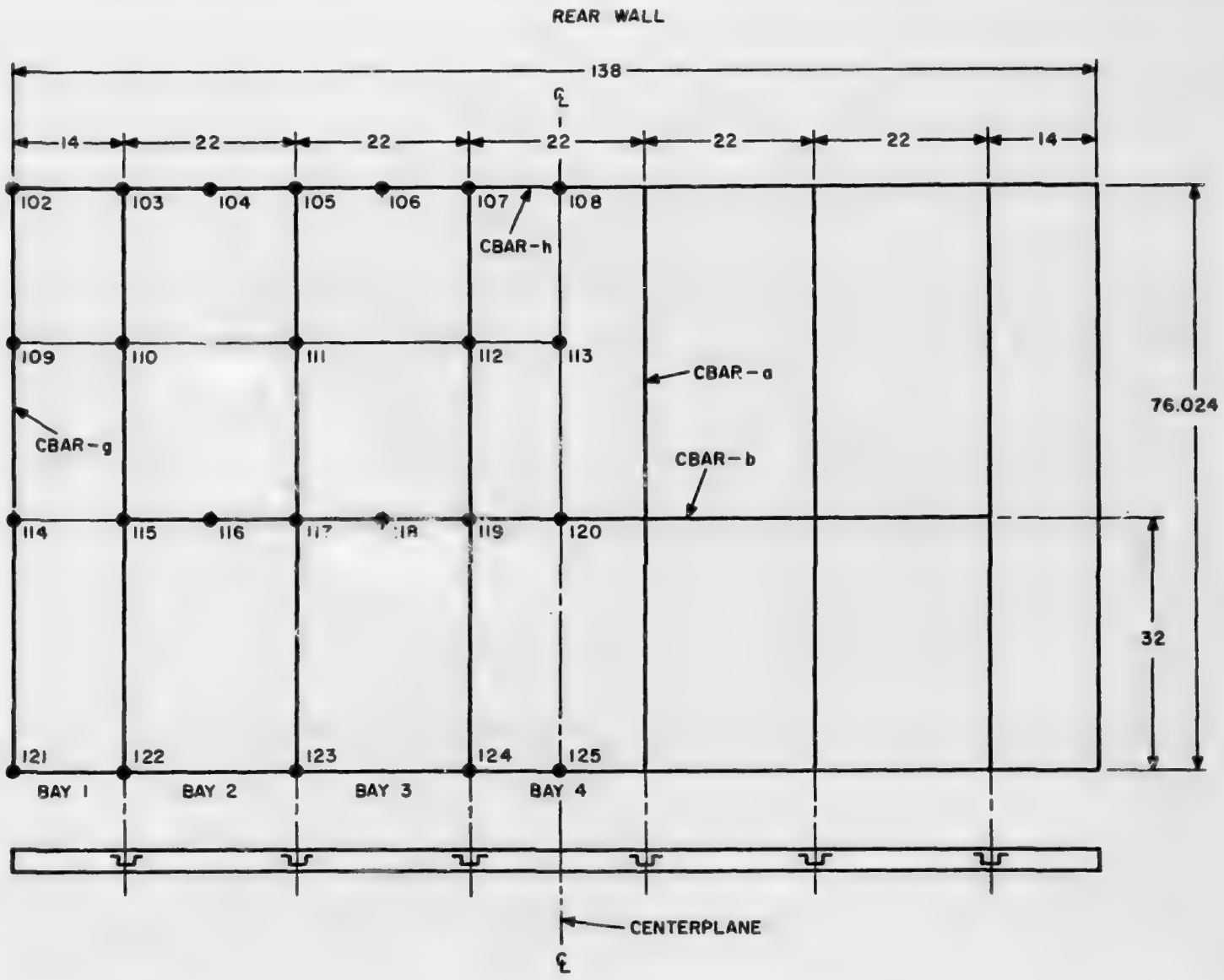

Figure 2.3 - Rear Wall Grid System

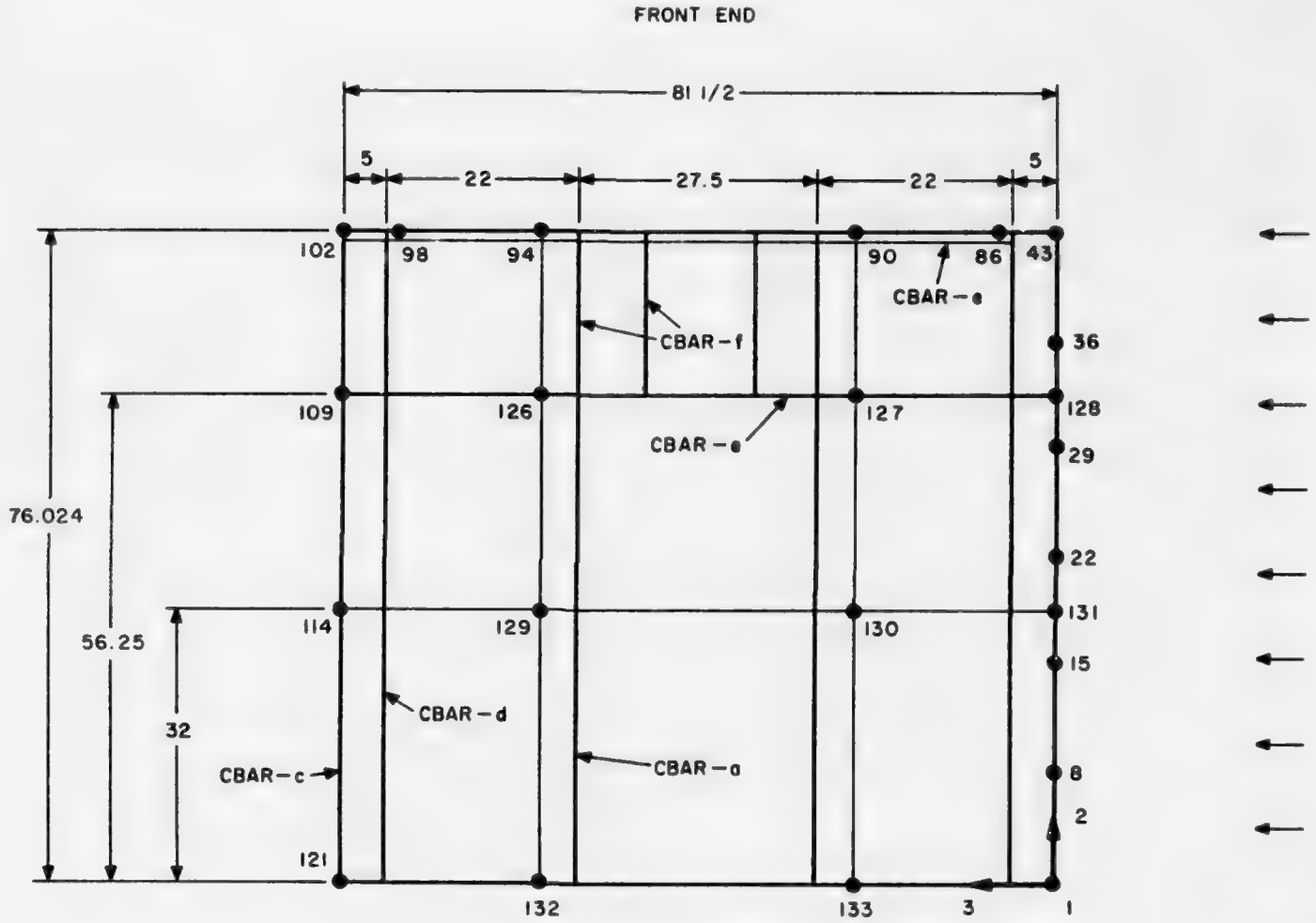

Figure 2.4 - End Wall Grid System

2.2 Loading Model

The loading on the shelter consists of a shock wave impinging normal to the surface of the front wall and subsequently enveloping the remaining shelter structure. The code SHELTR, which is described in Section 5 of Ref. 1, was used to determine the pressure loading on the structure and convert it to discrete forces acting at the grid points as a function of time. A SHELTR postprocessor program then reformatted the SHELTR tape output and constructed tables of the blast forces applied to the grid points at each time increment. The time dependent forces acting on the grid areas were punched on TABLED1 cards. TLOAD1 cards connected these loads with DAREA cards in order to transfer the load from the grid area to actual grid points on the shelter walls. A DLOAD card was then used as a superposition-type mechanism to load each surface as the sum of the grid point loads. The front wall loading was obtained from the code ASLOFF whose output was provided by BRL on tape. ASLOFF provides average overpressure predictions based on empirically derived equations relying on shock tube data, and accounts for rarefaction waves originating at the shelter edge.

The shock strength selected had an incident overpressure of 2.61 psi, corresponding to a test level of interest in the DIAL PACK field test.

2.3 Numerical Results

Three basic cases of the complete shelter were run with the NASTRAN direct transient solution rigid format. The first case excluded the cable forces, the second included the cable forces but assumed a zero preload ($F_0 = 0$), and the third considered a preload of $F_0 = 2000$ lb in each cable. The $F_0 = 2000$ lb case was considered an upper bound for practical considerations and represents a static prestress level in the cable of approximately 18,000 lb/in^2.

When the cables are pretensioned, the shelter-rack structure is in an initial static state of deformation prior to blast loading. To obtain this initial state of equilibrium, the NASTRAN static solution rigid format was run under the static force components of the 2000 lb cable forces at grid points 43 and 102. The displacements thus obtained at each grid point were input as initial conditions on TIC cards to be used for the dynamic response due to the blast loads.

The dynamic response was obtained for each case mentioned above for the 2.61 psi incident shock overpressure of the DIAL PACK field test. The responses of interest are at grid points 13 and 27 on the front wall (Fig. 2.1) and grid point 64 on the front rack (Fig. 3.3). These points correspond to locations where accelerations were measured during the DIAL PACK test. Examination of the plotted NASTRAN outputs for the three cases revealed that the displacement time histories at grid points 13, 27 and 64 were virtually unaffected by the cable forces, the responses being almost identical for each of the three cases run. The acceleration time histories were also identical for each case at grid points 13 and 27. At grid point 64, the accelerations for the no-cable case and the $F_0 = 0$ case were fairly close and the $F_0 = 0$ and $F_0 = 2000$ lb cases

were practically the same. Therefore, insofar as the displacement and acceleration responses at these grid points are concerned, the influence of the cables was unimportant.

The responses on the front wall and front rack obtained with the complete shelter model are compared with those obtained, at the same grid points, with the simpler structural model of Ref. 1, designated as Stage 2 with boundary condition set 3. The Stage 2 model consists only of the front wall and front racks and the boundary conditions (set 3) assume the bases of the wall, racks and the vertical edges of the wall are clamped and the tops of the racks are connected to the top (free) edge of the wall. Since the effects of the cables were unimportant in the three complete shelter cases, the $F_0 = 0$ case was selected as representative for comparison with the simpler Stage 2 model results.

The displacements and accelerations obtained by the complete shelter model and the Stage 2 model on the front wall at grid points 13 and 27 are compared in Figs. 2.5 - 2.8. It is seen that there are small differences in the peak amplitudes and in the basic frequency content of the time histories for displacements as well as accelerations. The maxi-max shock spectra* obtained from the acceleration time histories for each of these two models at grid points 13 and 27 are compared in Figs. 2.9 and 2.10. There, also, small differences exist between the spectra based on the complex and the simpler structural model acceleration responses.

The front rack responses at grid point 64 are compared in Figures 2.11 and 2.12. Overall, these responses compare favorably with respect to peak amplitudes and the frequency content of the time histories. The corresponding acceleration shock spectra, shown in Fig. 2.13, also compare closely. The sharp peaks noted in the shock spectra at frequencies of 1000-3000 cps would be smoothed out considerably if damping had been used in generating the shock spectra.

Examples of the displacements at the cable attachment point, grid point 43, are shown in Figs. 2.14 and 2.15 for components u_2 and u_3. The values at t=0 for $F_0 = 2000$ lbs correspond to u_{02} and u_{03} in Eqs. (A.13). In these figures, the cable preload shows a more significant effect on the u_2 displacement than on u_3. In general, the effects of the cables were pronounced only at the attachment points, and mostly in the acceleration response.

*The maxi-max shock spectrum is the maximum absolute acceleration experienced by a single degree of freedom oscillator as a function of its own natural frequency in response to a shock or vibration input.

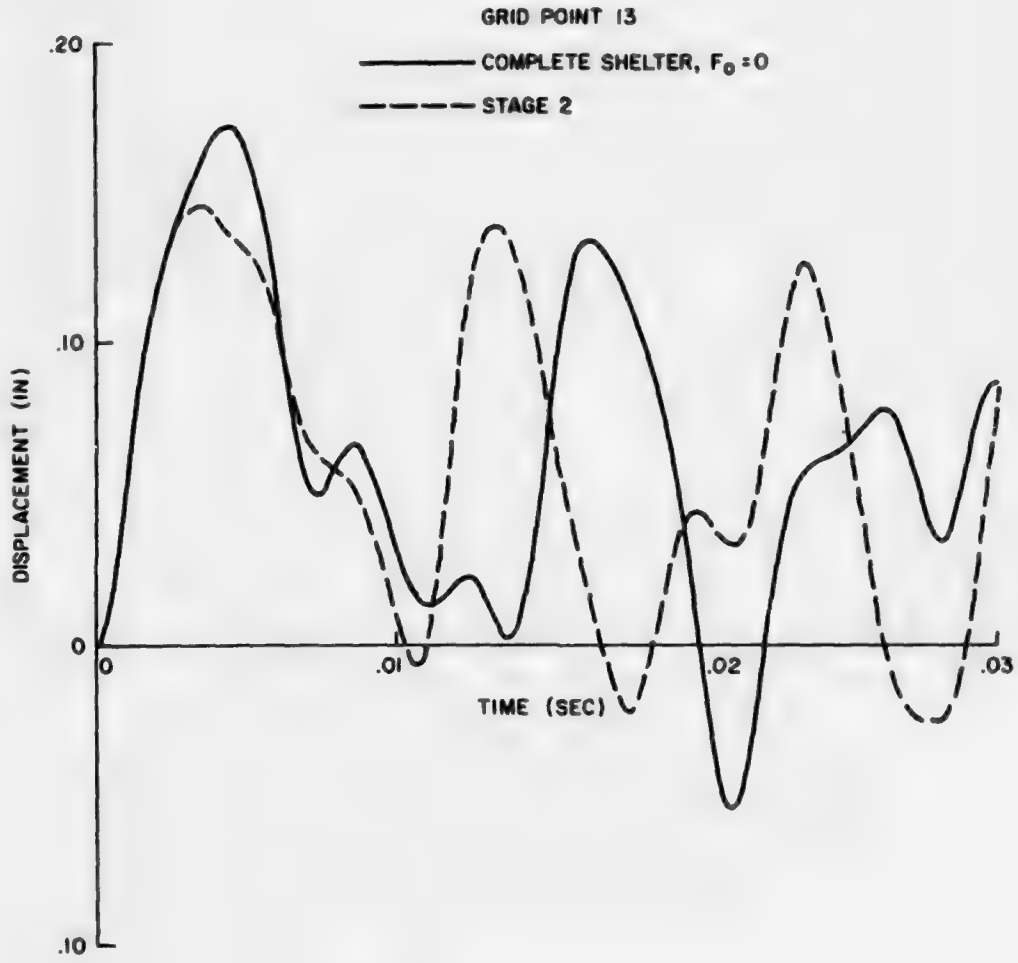

Figure 2.5. Comparison of Front Wall Displacement Histories

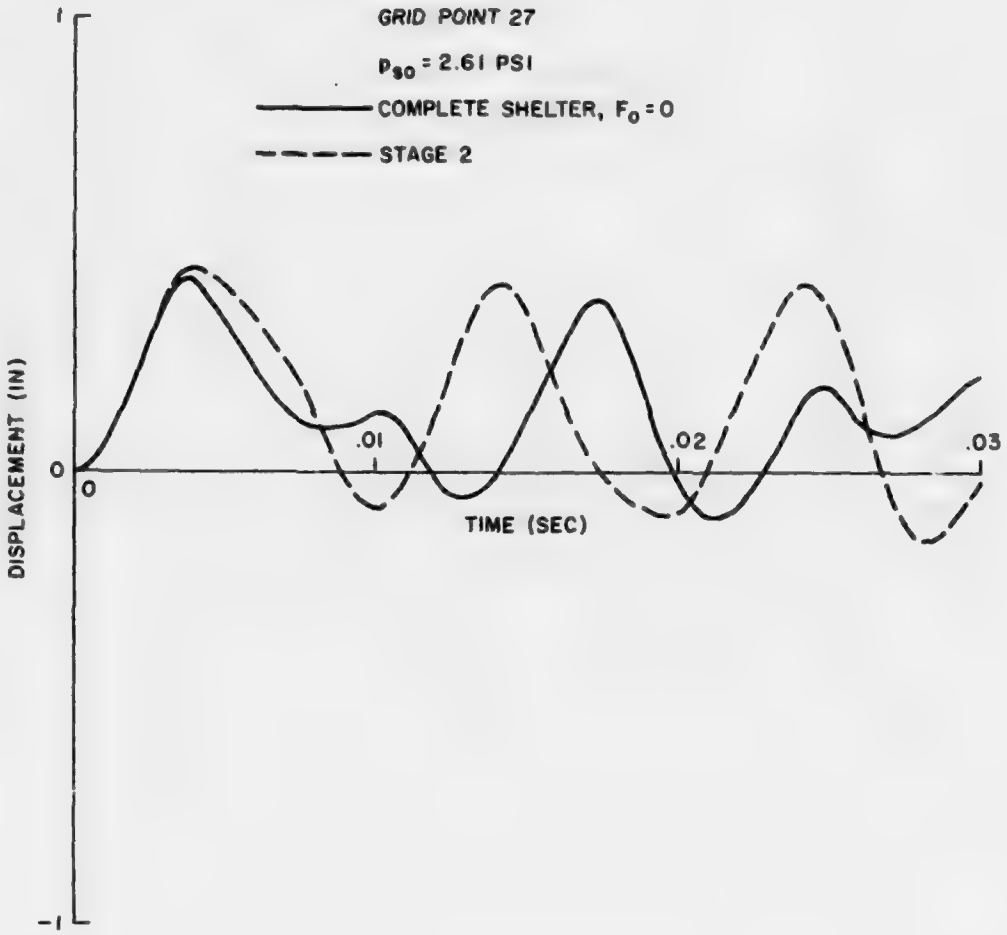

Figure 2.6. Comparison of Front Wall Displacement Histories

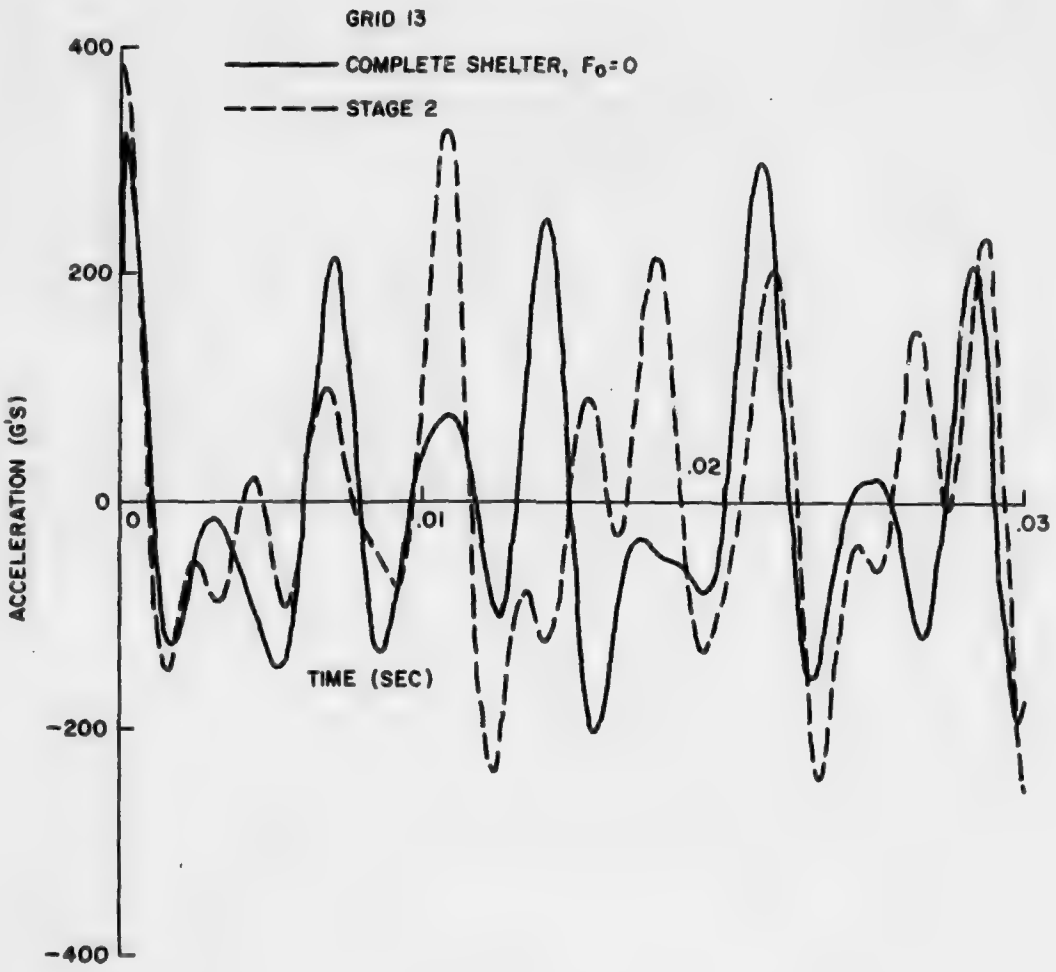

Figure 2.7. Comparison of Front Wall Acceleration Histories

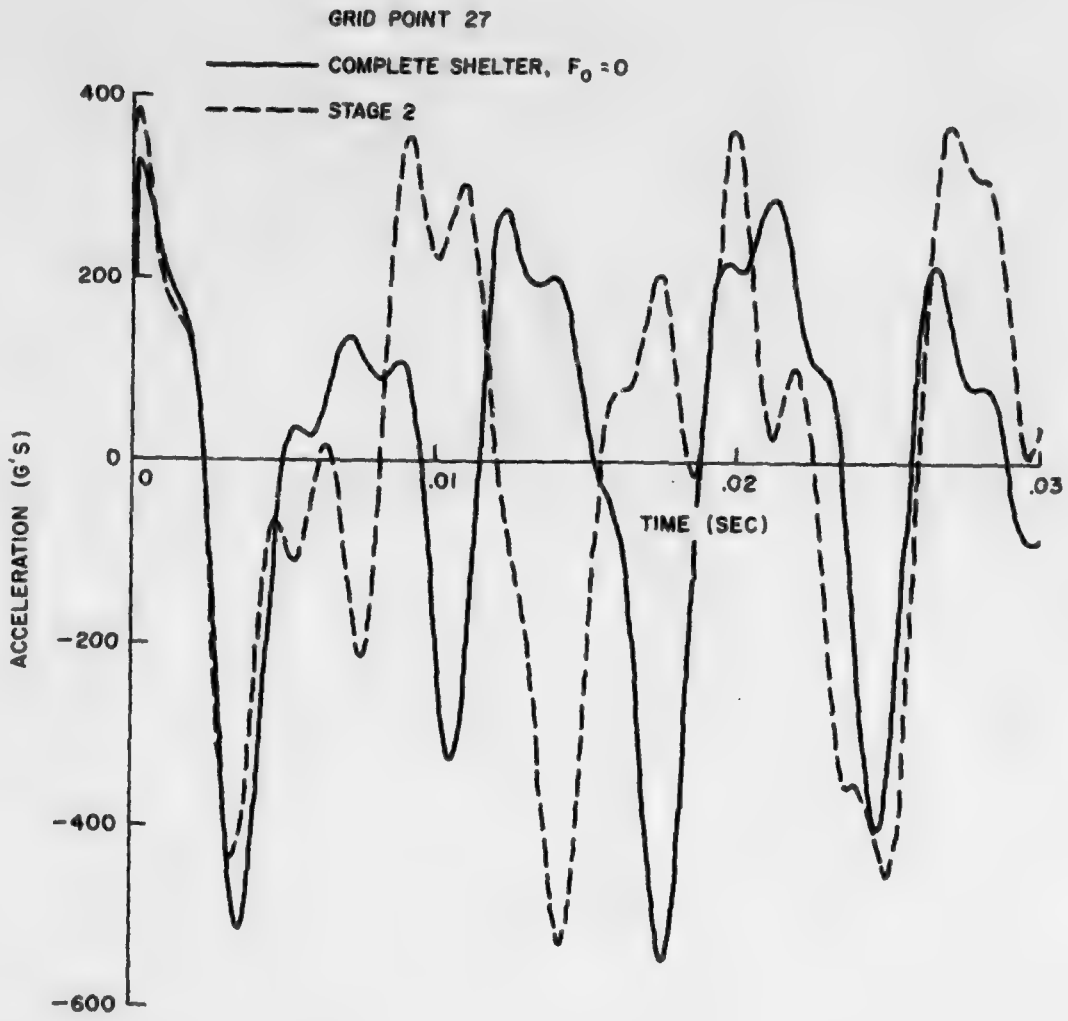

Figure 2.8 Comparison of Front Wall Acceleration Histories

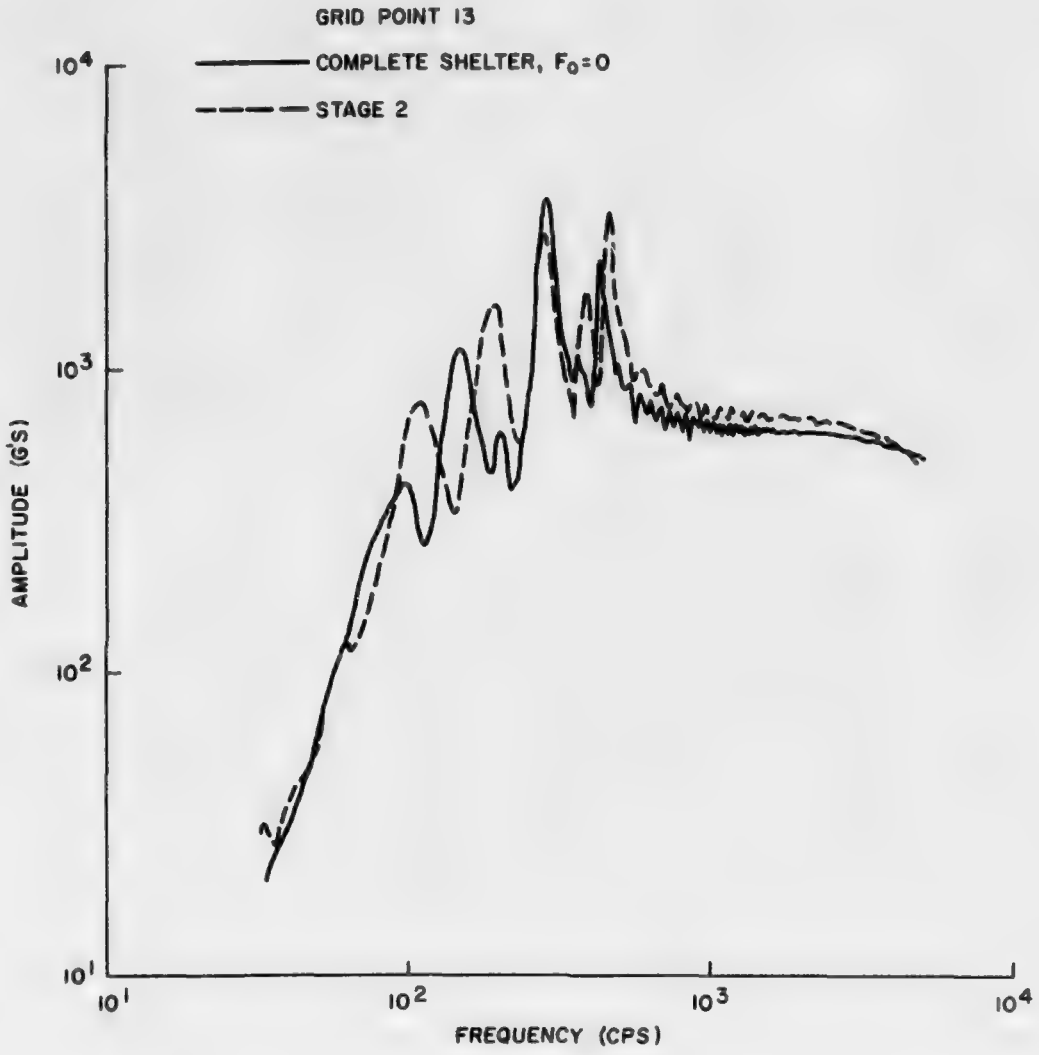

Figure 2.9. Comparison of Front Wall Acceleration Shock Spectra

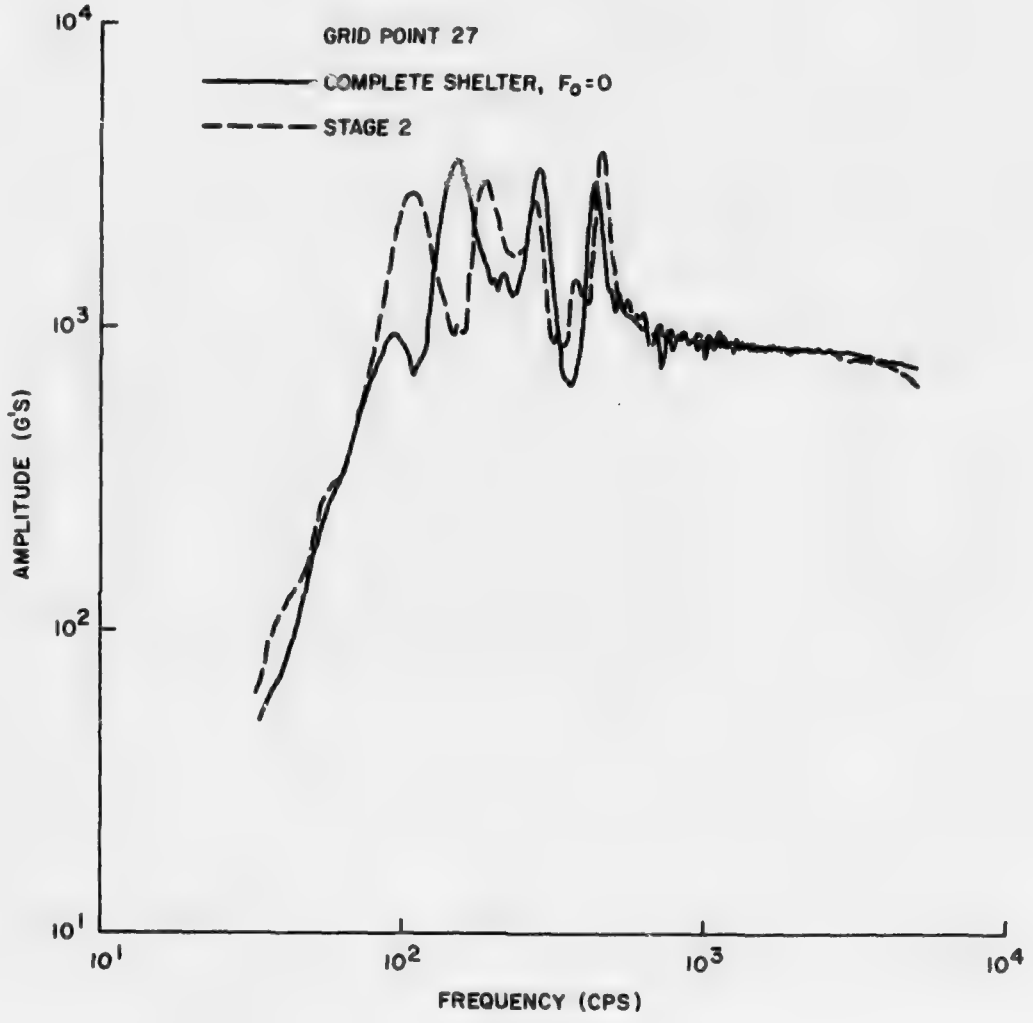

Figure 2.10. Comparison of Front Wall Acceleration Shock Spectra

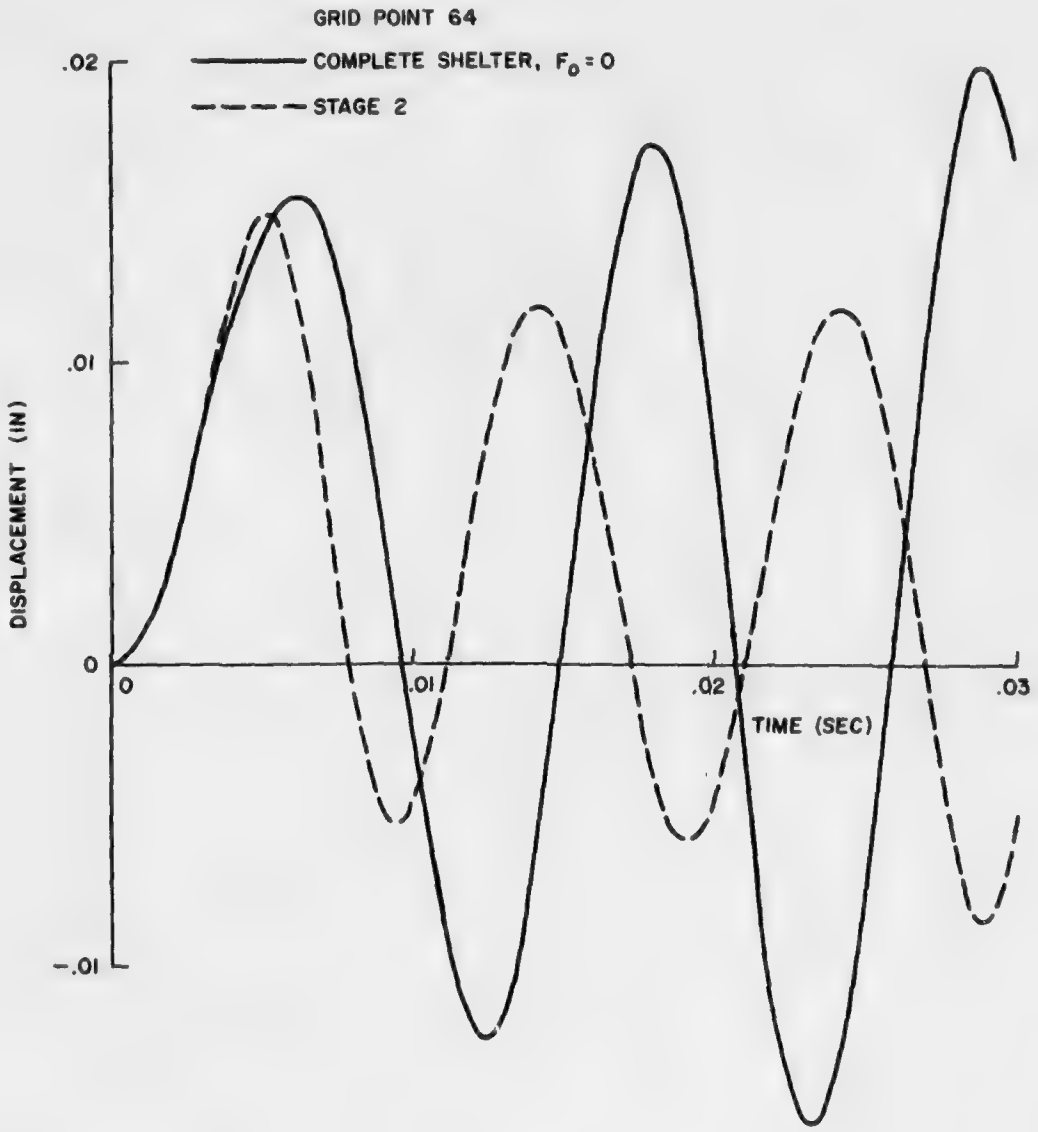

Figure 2.11. Comparison of Front Rack Displacement Histories

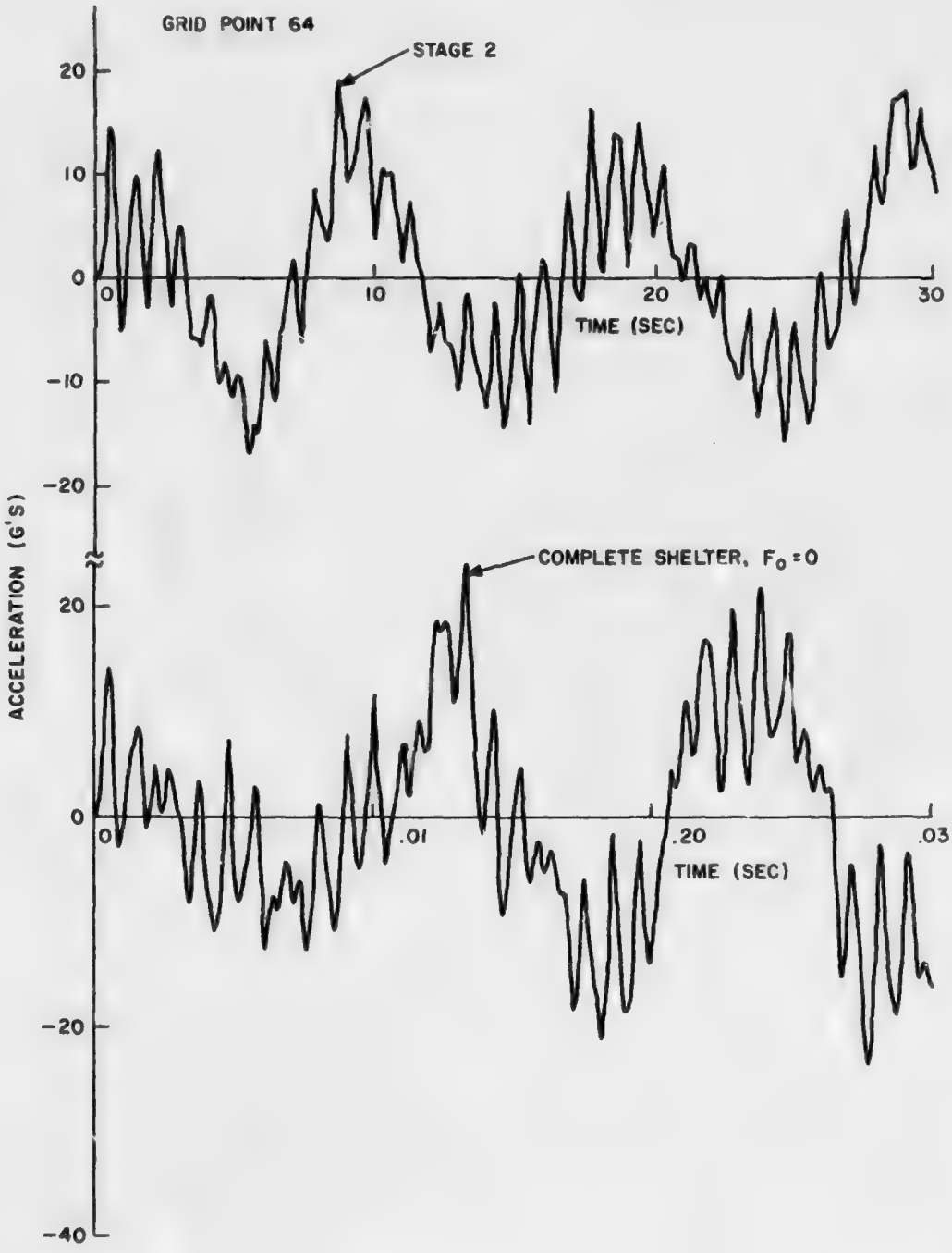

Figure 2.12. Comparison of Front Rack Acceleration Histories

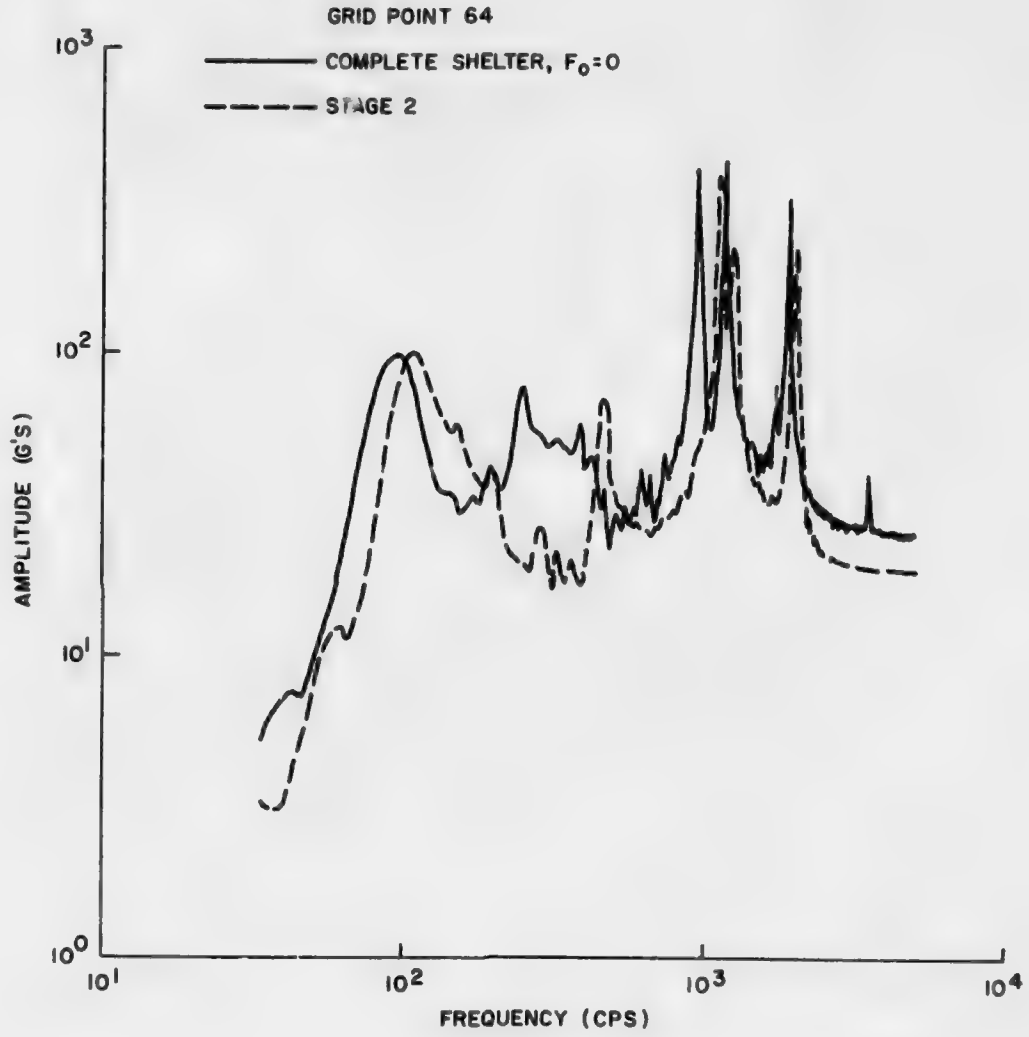

Figure 2.13. Comparison of Front Rack Acceleration Shock Spectra

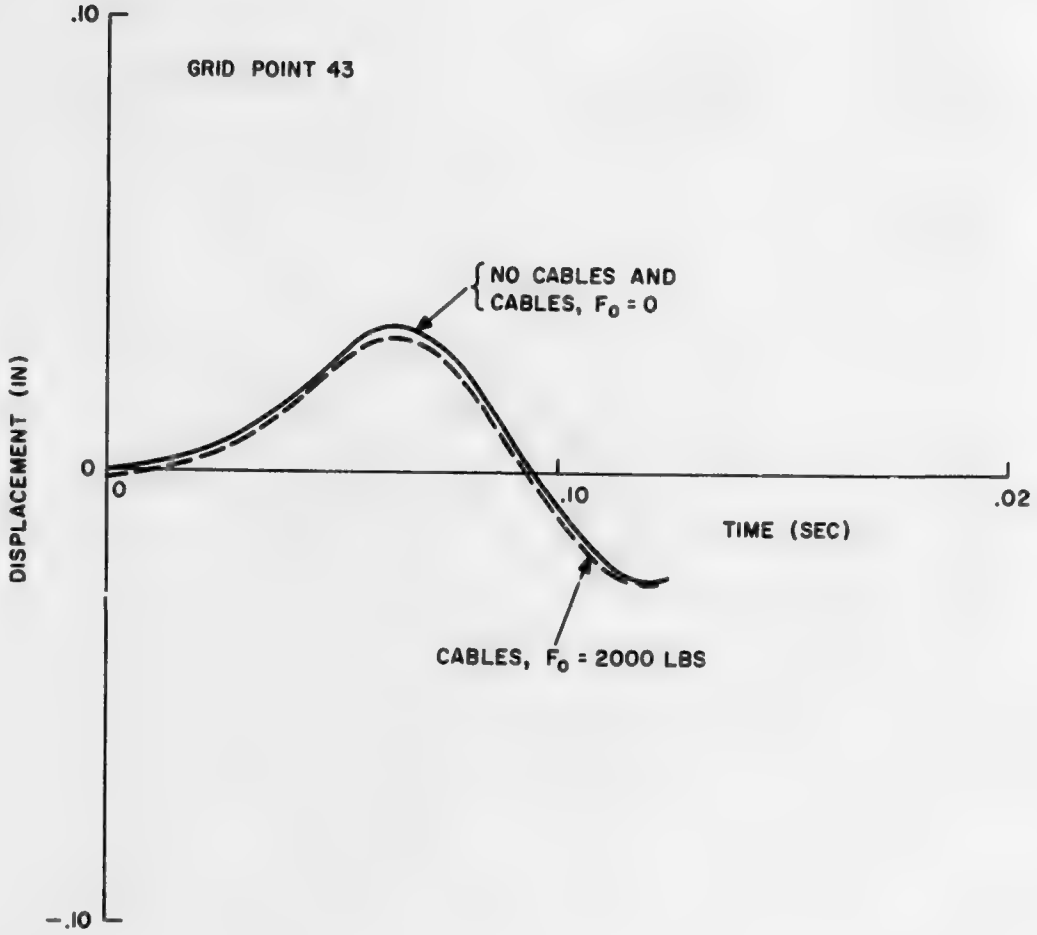

Figure 2.14. Effect of Cables on Attachment Point Displacement History, Direction 3

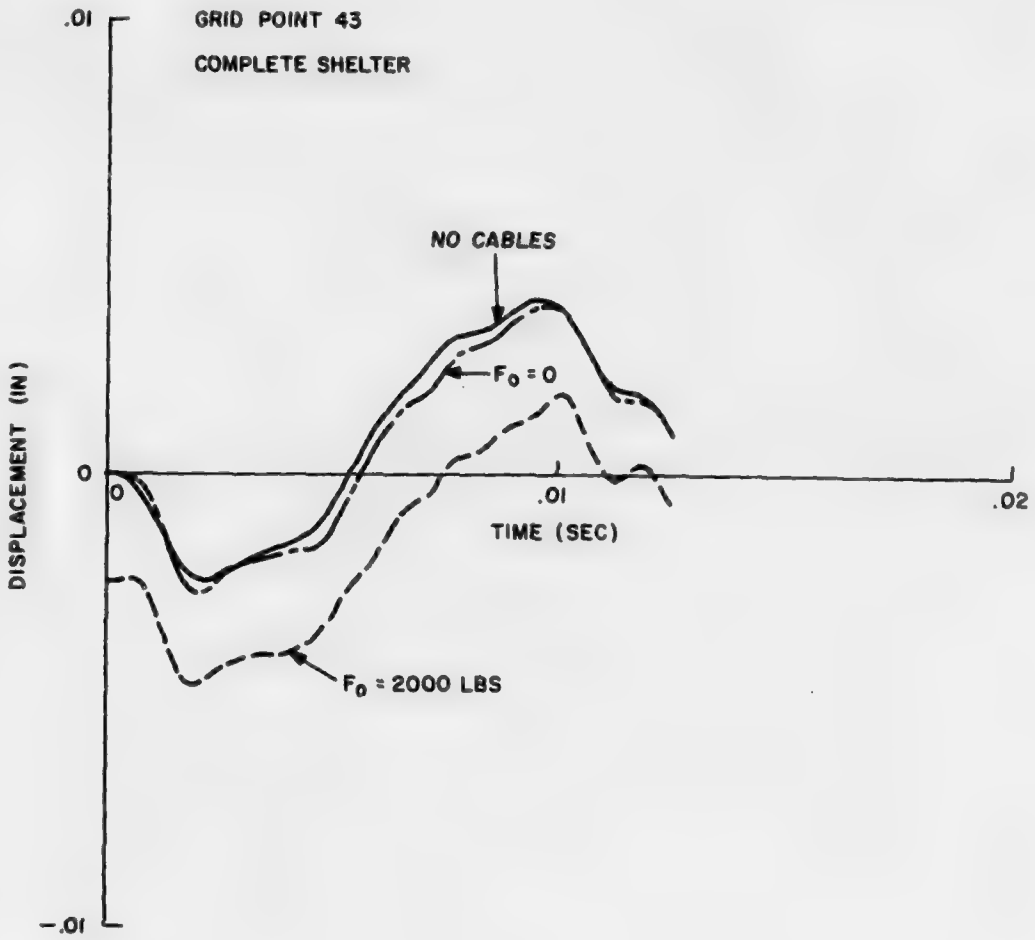

Figure 2.15. Effect of Cables at Attachment Point Displacement History, Direction 2

The maximum cable force attained during the blast response for F_0 = 2000 lbs occurs when t is approximately 6.5 msecs. At this time, the displacement components at grid point 43 are

$$u_1 = 1.182 \times 10^{-3} \text{ in.}$$

$$u_2 = -9.29 \times 10^{-4} \text{ in.} \qquad (2.1)$$

$$u_3 = 2.98 \times 10^{-2} \text{ in}$$

Referring to Appendix A and using Eqs. (A.6, A.14) and (2.1), the total cable stretch $|T|$ is 0.09983 in. and the cable force components applied to grid point 43 at 6.5 msecs are, using Eqs. (A.5) and (A.12),

$$F_1 = -1013.4 \text{ lb}$$

$$F_2 = -1605.1 \text{ lb} \qquad (2.2)$$

$$F_3 = -1773.5 \text{ lb}$$

resulting in a total cable force of 2598 lb, 598 lb above the preload value.

The shock spectra shown above were obtained from acceleration time histories of 30 msec duration. Figure 2.16 shows the typical effect on the shock spectrum when the acceleration time history was truncated at 12.5 msec. The shorter time history influenced the shock spectrum primarily at the lower frequencies, below 500 cps for this case. This is attributed to an insufficient number of cycles of the lower modes in the shorter time history. Referring to the time history in Figure 2.8 which was used to generate the spectra in Figure 2.16, it is seen that there is a lower mode of about 140 cps of which only one complete cycle was included in the truncated 12.5 msec time history. This points out the need for having a sufficiently long time history for the shock spectrum, even though the peak acceleration may occur at very early time.

2.4 Summary

The results for the three complete shelter cases considered indicate that the cable forces had a minor effect on the displacement and acceleration responses of the front wall and front rack. One major reason for this is that the substantial weight of the enclosed racks (3000 lb vs 1280 for the empty shelter) provides a significant portion of the resistance of the complete structural assemblage to the blast. Another major factor are the clamped boundary conditions at the shelter floor. The combination of these factors restricted the influence of the cable forces mainly to the local regions near the cable attachment points. In the real situation encountered in the field tests, the primary function of the cables is to inhibit rigid body motions and prevent overturning.

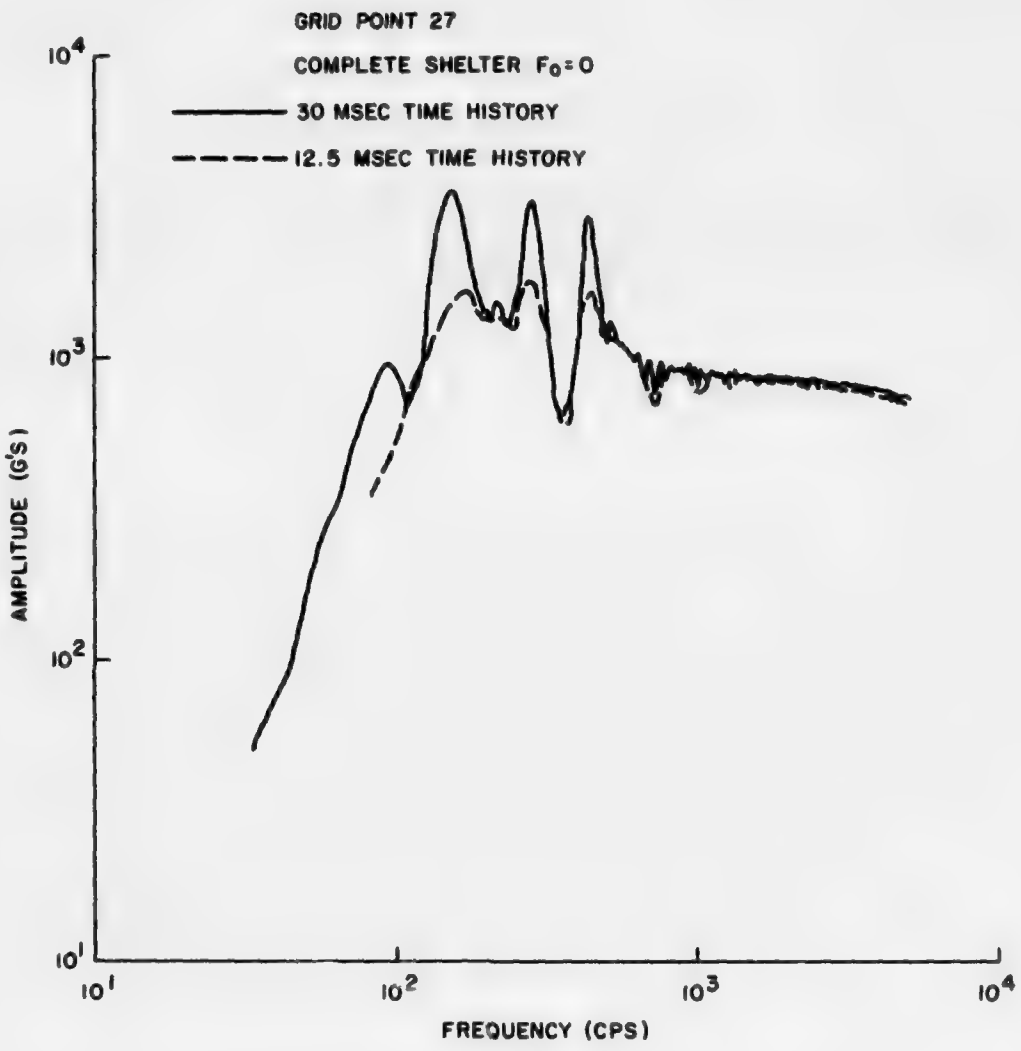

Figure 2.16. Typical Effect of Duration Acceleration Time History on Shock Spectrum

The comparisons between the complete shelter results and those obtained by using the simpler model consisting only of the front wall and front racks showed minor differences in the basic character of the responses. Thus, the addition of the remaining shelter structure to the simpler model offers no advantages for the responses of interest here and provides a penalty in the form of additional degrees-of-freedom. Of course, the more complete model provides the response of the complete system (roof, rear walls, etc.) which the simpler model cannot. The unimportance of the remaining structure is attributed to the predominant rack weight mentioned above. This conclusion should not be generalized to other shelter systems since they may incorporate racks which are lighter and less stiff than those considered in the present application.

In Ref. 1, comparisons were made between the DIAL PACK test data and the analytical results based on the Stage 2 structural model. It was shown there that in general the predicted front wall accelerations were consistent with the test data but that the predicted front rack accelerations were substantially lower than the test values. Since it was shown in this section of the report that the front wall and front rack responses as obtained by the complete shelter model and the Stage 2 model were substantially the same, then the comparison of the complete shelter responses with the test data will be the same as shown for the simpler model in Ref. 1. The DIAL PACK test data is presented in Section 3 of this report, where further comparisons are made with the Stage 2 model incorporating more refined finite element models of the front rack structure.

SECTION 3

EFFECTS OF RACK MODEL MODIFICATIONS

3.1 Introduction

The comparison of accelerations measured on the rack structure during the DIAL PACK event with those obtained analytically with the NASTRAN model in Ref. 1 indicated that the analytical peaks were considerably lower than the measured data. Several factors may contribute to this discrepancy, such as the influence of the shelter rigid body response, gage selection and placement and details in the analytical modeling. This section investigates the effects of improvements in the analytical structural model of the racks employed in NASTRAN. More detailed models of the racks are developed by adding more grid points and increasing the number of structural plate and beam elements and consequently the degrees of freedom. These refinements introduce higher frequencies which can affect the amplitude and frequency of the desired response. The original rack model, by nature of its reduced structural detail and fewer degrees-of-freedom in essence "filtered" out the influence of the higher response modes.

This filtering effect is investigated by studying three rack modifications of increasing complexity, MOD-1, MOD-2 and MOD-3. Each of these modified rack models replaced the original rack model in the Stage 2 model described in Ref. 1 with boundary condition set 3. It will be recalled that the Stage 2 model comprises the front wall and the front racks. In boundary condition set 3 the bases of the racks and the base of the front wall are clamped, the tops of the racks are connected to the top of the front wall which is unrestrained and the vertical edges of the front wall are clamped.

3.2 Modeling

A schematic of a single equipment rack is shown in Fig. 3.1 and a layout is given in Fig. 3.2 of the bolt retainer rails, the panel mounting angles and the vertical side supports, all of which were modeled as beam members. Reference 1 (Subsection 4.3) should be consulted for more details on the racks.

Figure 3.3 shows the grid system used for the original rack model of Ref. 1. The base of the racks is clamped and the racks are rigidly connected to the front wall with multipoint constraint conditions at grid points 59-61, 71-73 and 77-79. The blast load is transferred from the front wall to the front racks at these grid points. The grid system in Fig. 3.3 shows the connectivity points for all plate and beam elements. Thirty-six grid points were used on the racks and 49 for the front wall for a total of 85 for the complete Stage 2 model

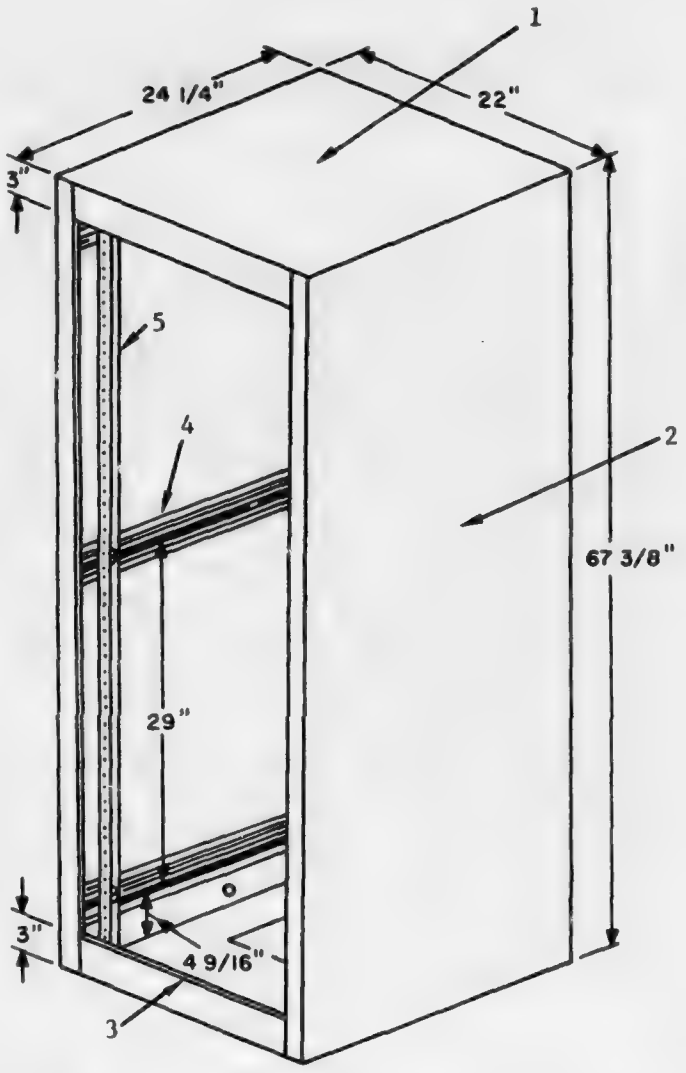

Part No.	Name	Material	Quantity
1	Top	.104 Steel	1
2	Sides	.059 Steel	2
3	Bottom	.104 Steel	1
4	Bolt Retainer Rails	.104 Steel	6
5	Panel Mounting Angle	.187 Steel	2

Figure 3.1 - Equipment Rack Dimensions

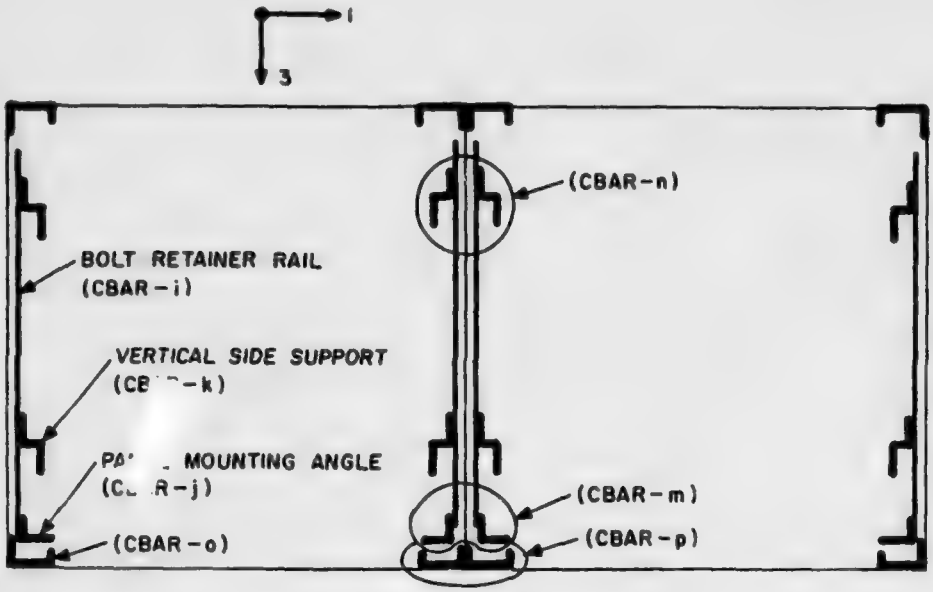

TOP VIEW

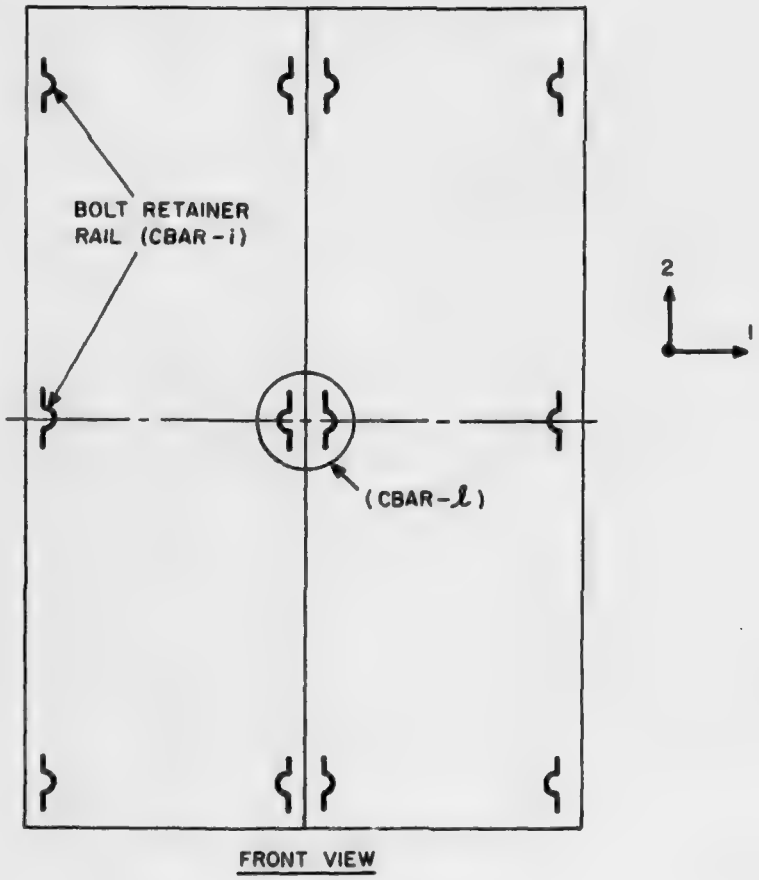

FRONT VIEW

Figure 3.2 - CBAR Cross-Section Schematic for Front Racks

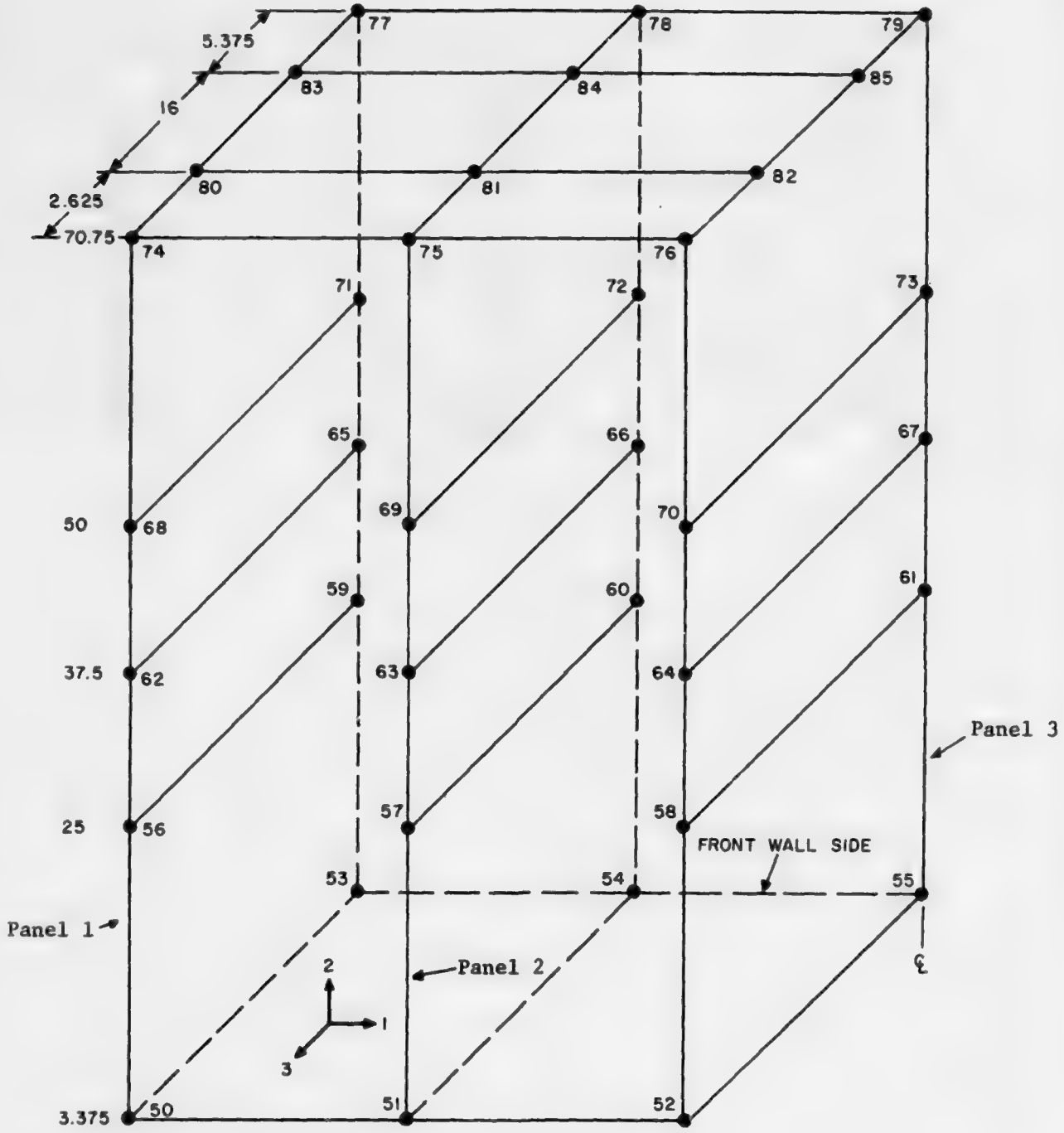

Figure 3.3. Original Front Racks Grid System

The grid system for the plate elements of MOD-1 is shown in Fig. 3.4 and the grid system for the beam elements is shown in Fig. 3.5. The properties of the plate elements comprising the side walls and the tops of the racks (CQUAD2) and of the beam members (CBAR i through p) are described in Ref. 1. MOD-1 contains more plate elements for the side walls than the original rack model, with Panel 3 having a finer grid system than Panels 1 and 2. A finer grid mesh is desirable in Panel 3 since it contains grid point 92 which corresponds to an accelerometer location*. In addition, a separate grid system was established for the beam elements of MOD-1 (Fig 3.5) which conforms more to the actual structural layout and utilizes more beam elements than the original model. Referring to Table 3.1, MOD-1 has approximately twice as many plate and beam elements as the original model and 111 degrees-of-freedom compared to the original 51.

Four equipment shelves supporting lead sheets to simulate equipment weights were mounted on each rack. These shelves are more realistically located in the MOD-1 model than in the original model. Referring to Fig. 3.6, four shelves were supported horizontally and four vertically by the vertical side supports, with grid points 66, 69, 162, 163 supporting a pair of vertical shelves. In the original model of Fig. 3.3, the eight shelves were more crudely represented at grid points 68-79 (for the horizontal shelves) and grid points 50-61 (for the vertical shelves). In both rack models, only the mass of the shelf was represented at the indicated grid points by CONM2 mass data cards. A weight of 80 lbs was taken for each horizontal shelf and 90 lbs for each vertical shelf.

The second modification, MOD-2, is a simple extension of MOD-1 to include the stiffening effects of the shelves which heretofore had been neglected. A schematic of the shelf mounting arrangement is shown in Fig. 3.7. Beam elements were used to model the steel side mounting brackets to which the horizontal shelves were bolted and plate elements were used to model each steel shelf, as shown in Figs. 3.6 and 3.7. The vertically mounted shelves were bolted directly to the vertical side supports but were not connected to side mounting brackets; the remaining structural model of the racks for MOD-2 was otherwise identical to the arrangements shown in Figs. 3.4 and 3.5 for MOD-1.

The MOD-3 model further extends the MOD-2 model by incorporating more beam and plate elements in Panel 3 in the local region of grid point 92 as shown in Figs. 3.8 and 3.9. This results in an increase in the grid points to 204. Referring to Table 3.1, the degrees-of-freedom for MOD-3 are 163 compared to 51 for the original rack model. Except for the increase in grid points in Panel 3, no other differences exist between MOD-2 and MOD-3.

*Grid point 92 corresponds to grid point 64 of the original rack model.

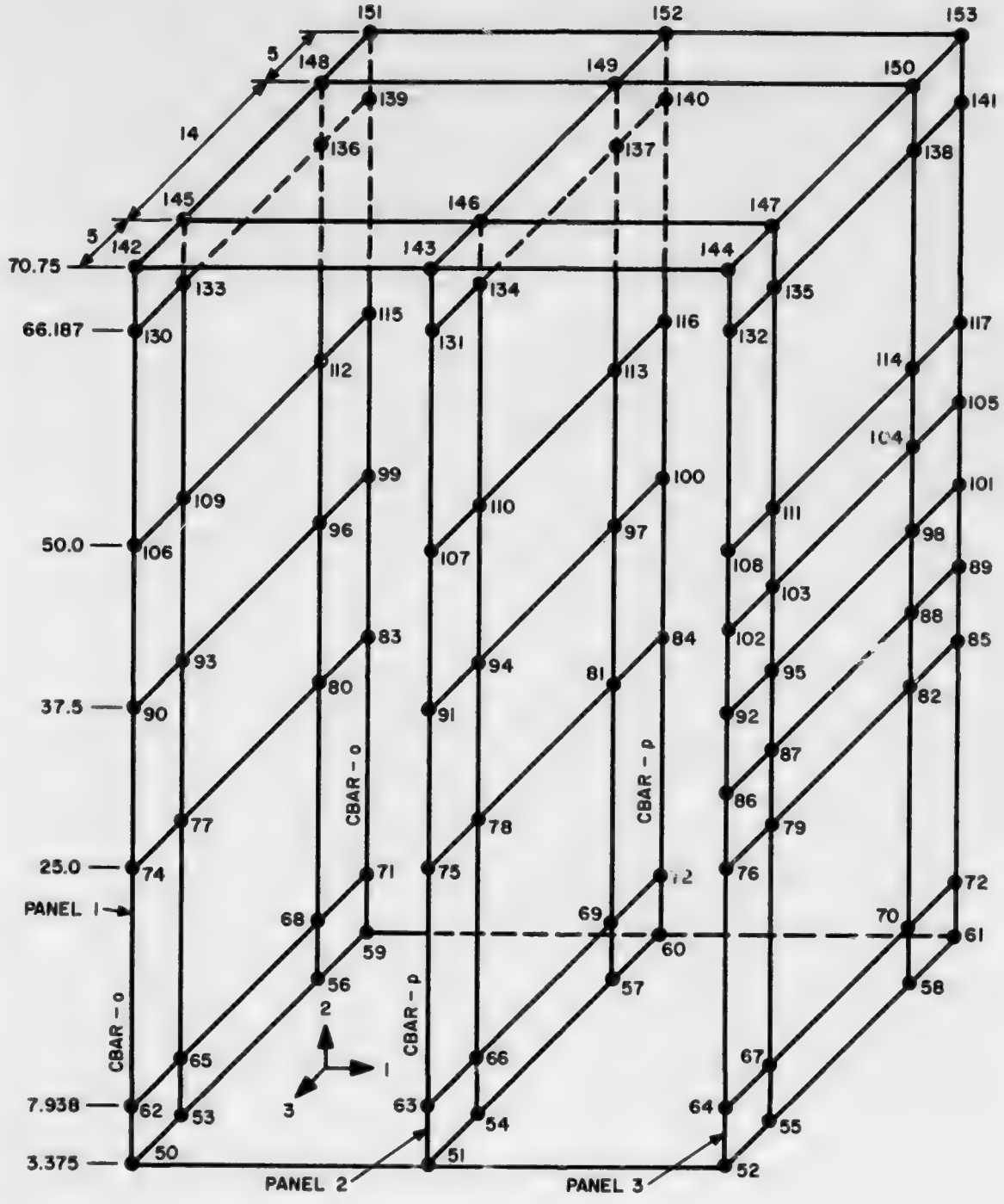

Figure 3.4. Grid System of Rack MOD-1 for Plate Elements

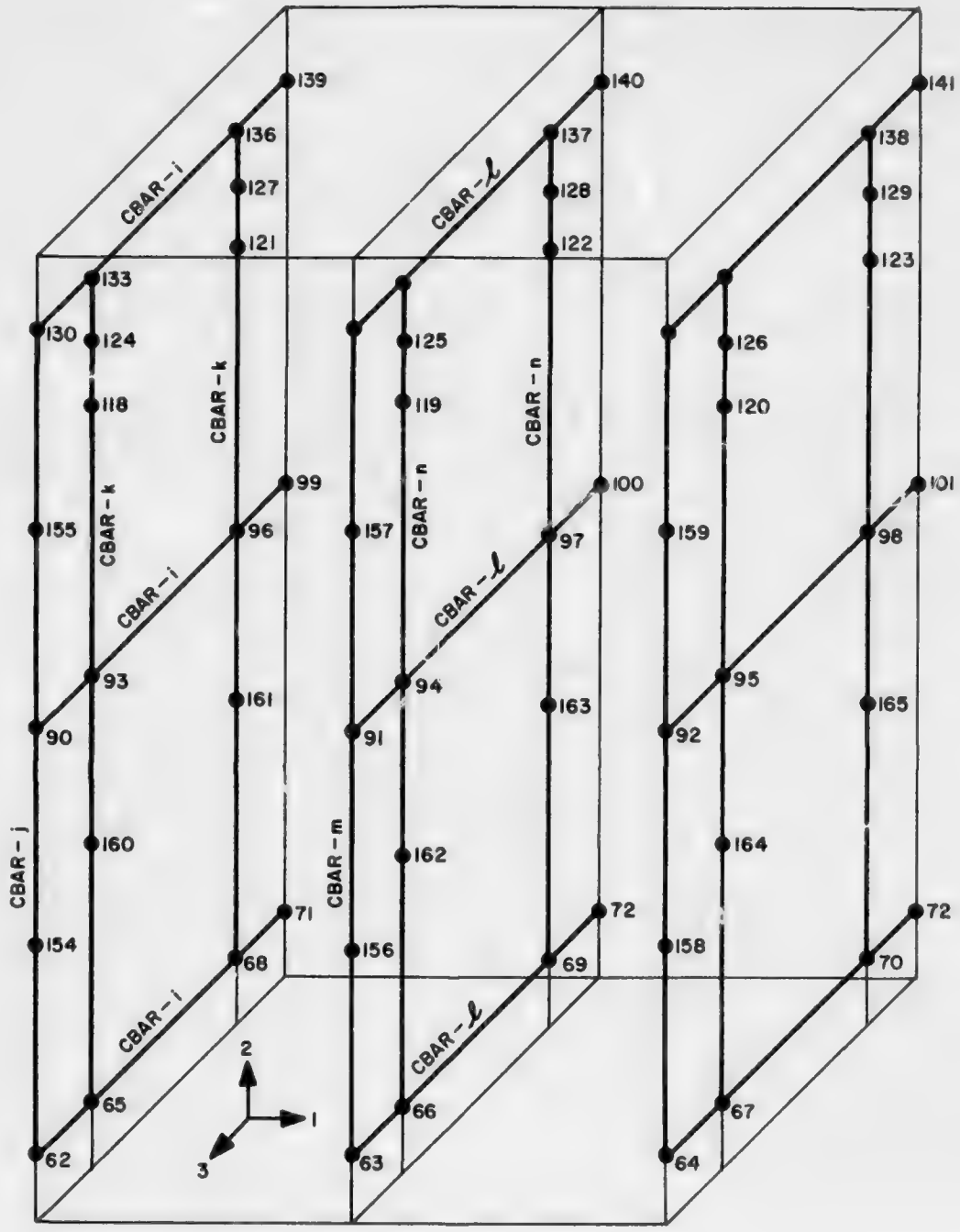

Figure 3.5. Grid System of Rack MOD-1 for Beam Elements

TABLE 3.1

SUMMARY OF RACK MODELS

Rack Model Case	Grid Points[1]	Structural Elements[2]		Degrees of Freedom
		Plate	Beam	
Original (Ref. 1)	85	54	79	51
MOD-1	165	102	143	111
MOD-2	165	110	151	111
MOD-3	204	134	169	163

Notes: (1) Each case includes 49 grid points for the front wall structure

(2) Each case includes 36 plate elements and 28 beam elements for the front wall structure.

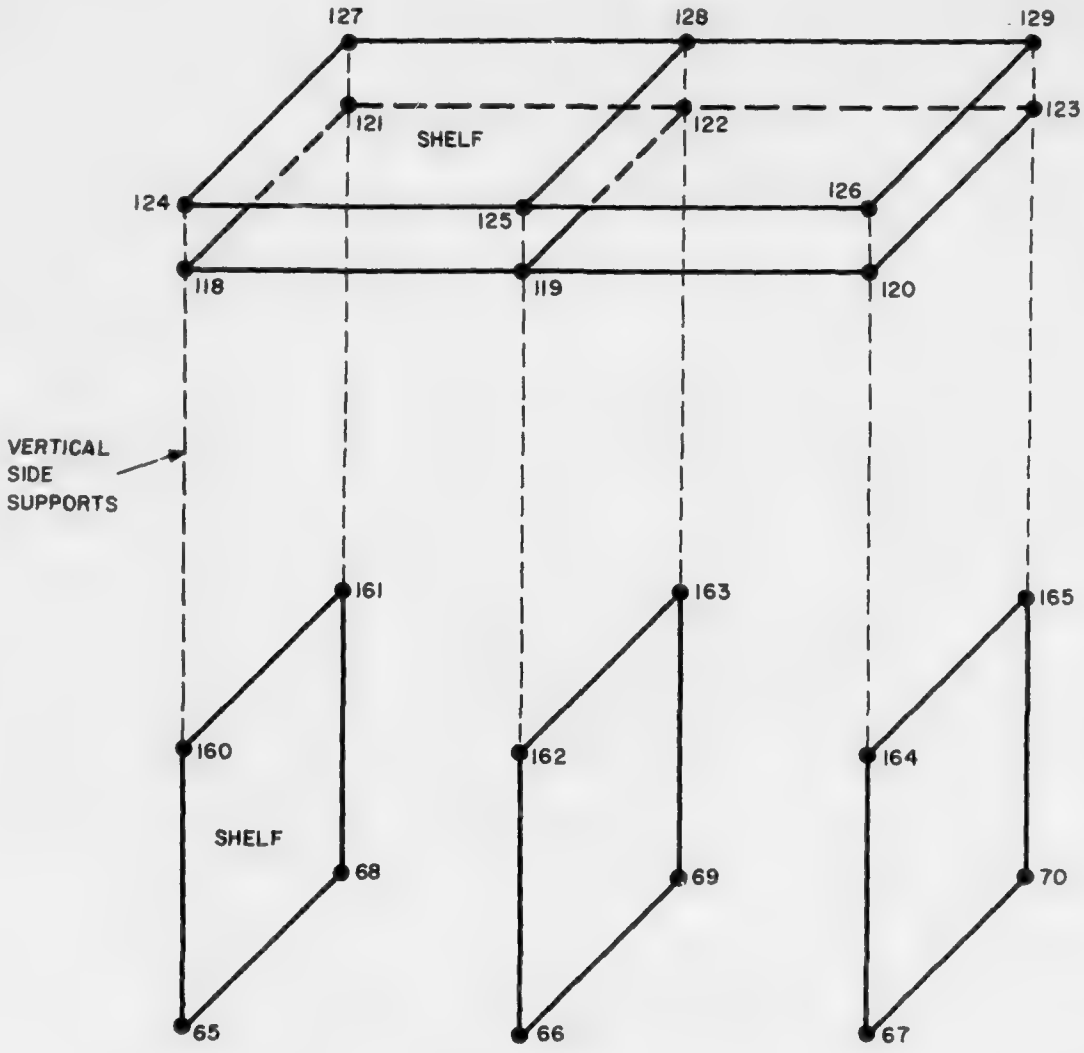

Figure 3.6. Arrangement of Horizontal and Vertical Equipment Shelves for MODS 1, 2 and 3.

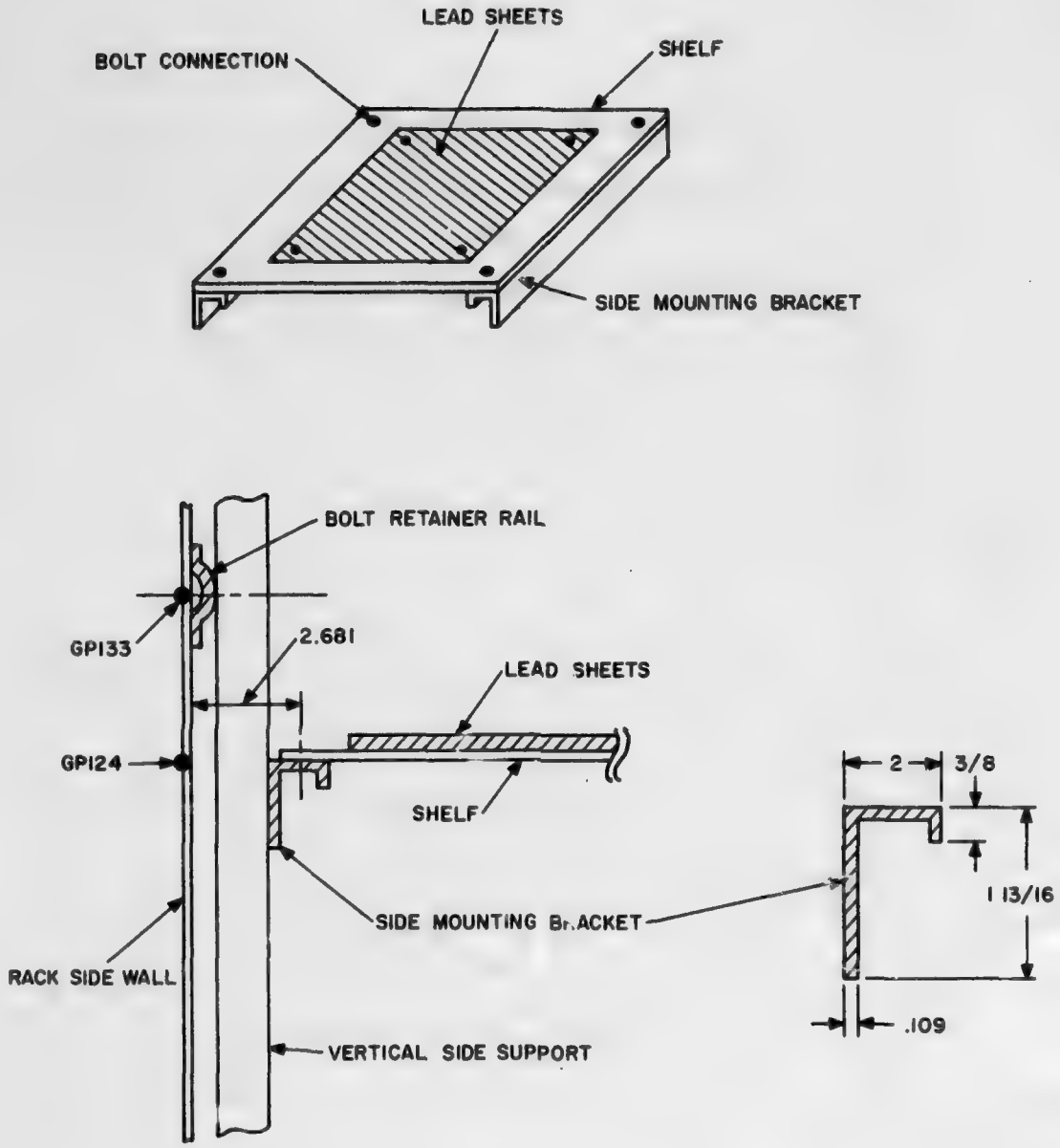

Figure 3.7. Detail of Horizontal Shelf Mount for MOD-2

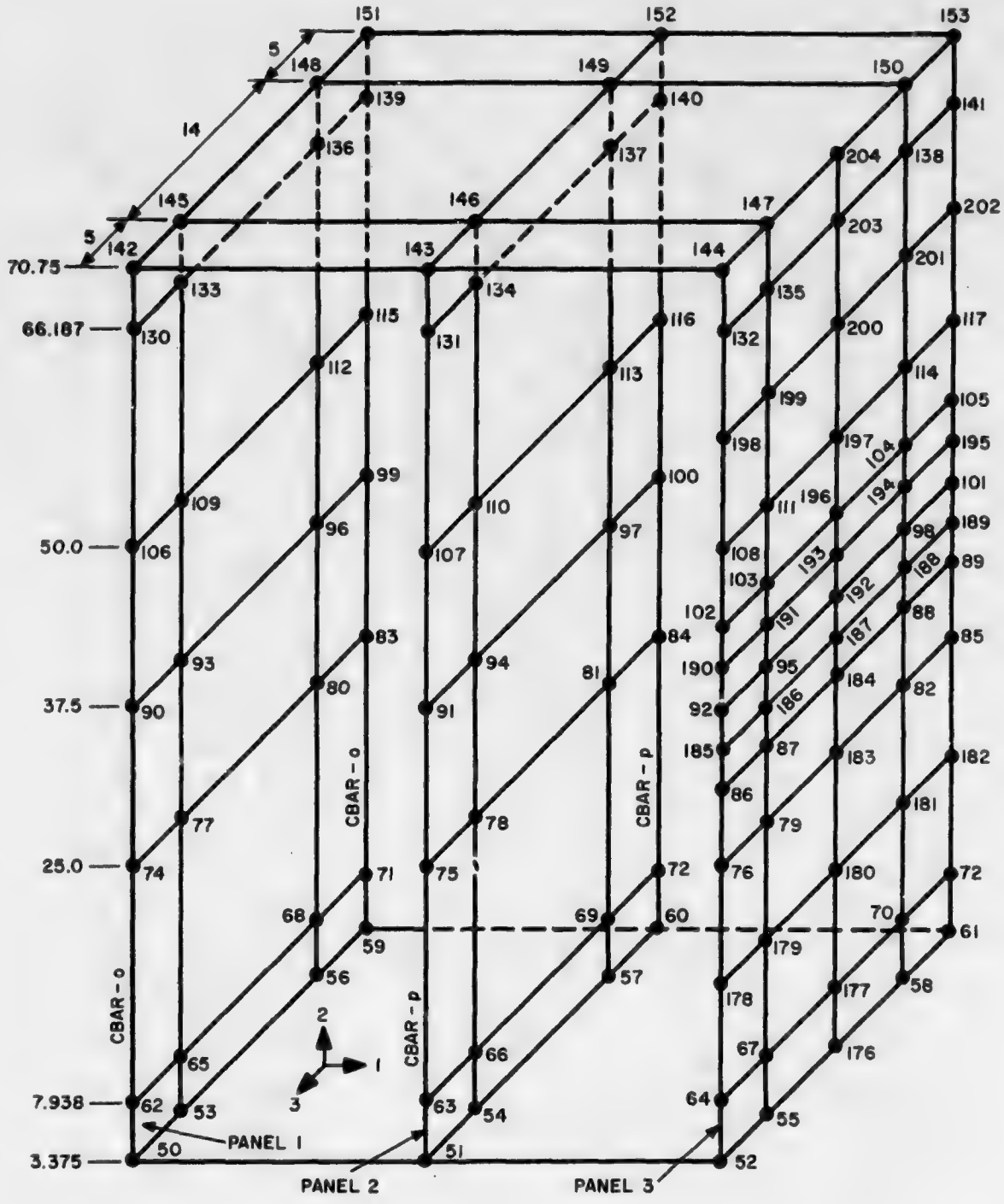

Figure 3.8. Grid System of Rack MOD-3 for Plate Elements

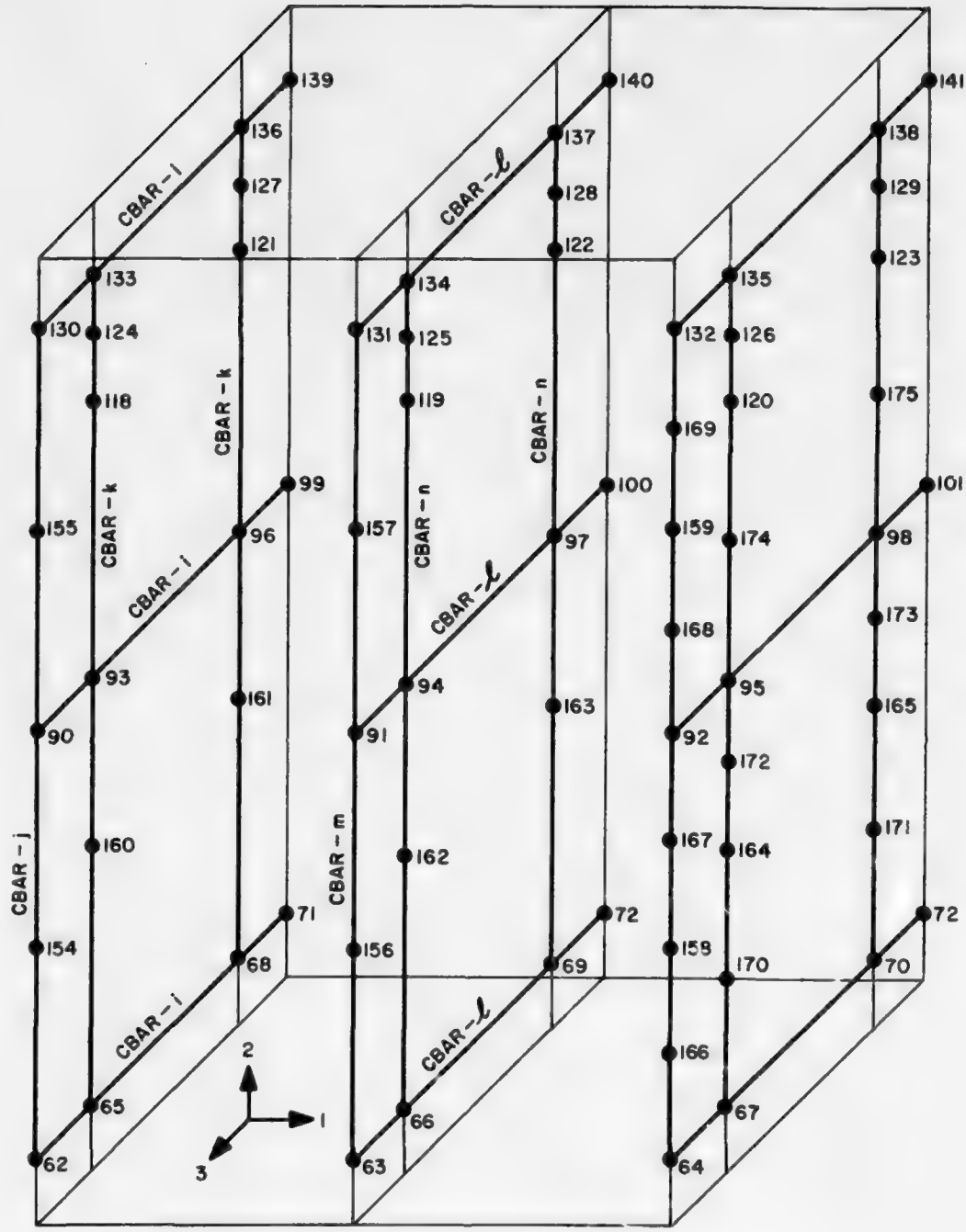

Figure 3.9. Grid System of Rack MOD-3 for Beam Elements

3.3 Results

Displacement and acceleration time histories were obtained by the direct transient response rigid format of NASTRAN. Prior to running NASTRAN, the code BANDIT was run to minimize the semi-bandwidth by resequencing the grid points for each MOD*. The resequenced data deck was then used in NASTRAN to obtain 30 msecs of response for each MOD. The incident overpressure for each case was 2.61 psi, as in Section 2.

The effect of each modification on the rack responses is of primary interest. However, front wall responses were also obtained to investigate their sensitivity to modifications of the rack model. The front wall responses are presented for grid points 13 and 27 and the rack responses for grid point 92, locations where accelerometers were mounted**.

The complete set of computer results showed that the front wall displacement and acceleration time histories at grid points 13 and 27 were virtually identical for MOD-1, MOD-2 and MOD-3. Therefore, the MOD-3 front wall responses were selected as representative of all three cases for comparison with the responses obtained with the original rack model of Ref. 1 and with the test data.

Comparisons of the front wall responses obtained with MOD-3 and with the original rack model are shown in Figs. 3.10 and 3.11 for displacements and in Figs. 3.12 and 3.13 for accelerations. It is noted that the rack model refinements had little influence on the displacements with regard to amplitude and frequency content over the full 30 msec response time. The accelerations display similar peaks and frequency content with slight shifts in phasing and the initial oscillation in the acceleration is essentially the same for both rack models. The rack model modifications, therefore, had little effect on the front wall responses and the acceleration responses showed a slightly greater sensitivity than the displacements.

As indicated in Ref. 1, comparison with the experimental front wall accelerations is difficult because the front wall data were clipped due to gage saturation (see Figs. 3.14 and 3.15). On the basis of extrapolation, though, the front wall test data and the analytical responses appear consistent in the level of response and display somewhat similar frequencies. The shock spectra for the two rack models are compared in Figs. 3.16 and 3.17, which also includes the experimental spectra based on the time histories in Figs. 3.14 and 3.15. Due to the similarities in the acceleration time histories for the original and modified rack models, the resulting shock spectra are also very similar. The experimental spectra, however, are lower which is consistent with the clipped time history data. Had the data not been clipped, the shock spectra would be higher, but the degree of agreement with the analytical spectra in Figs. 3.16 and 3.17 would be conjectural at the present time.

---

*This was also done for the complete shelter in Section 2.

**Experimental displacement time histories were not available for comparisons with NASTRAN results.

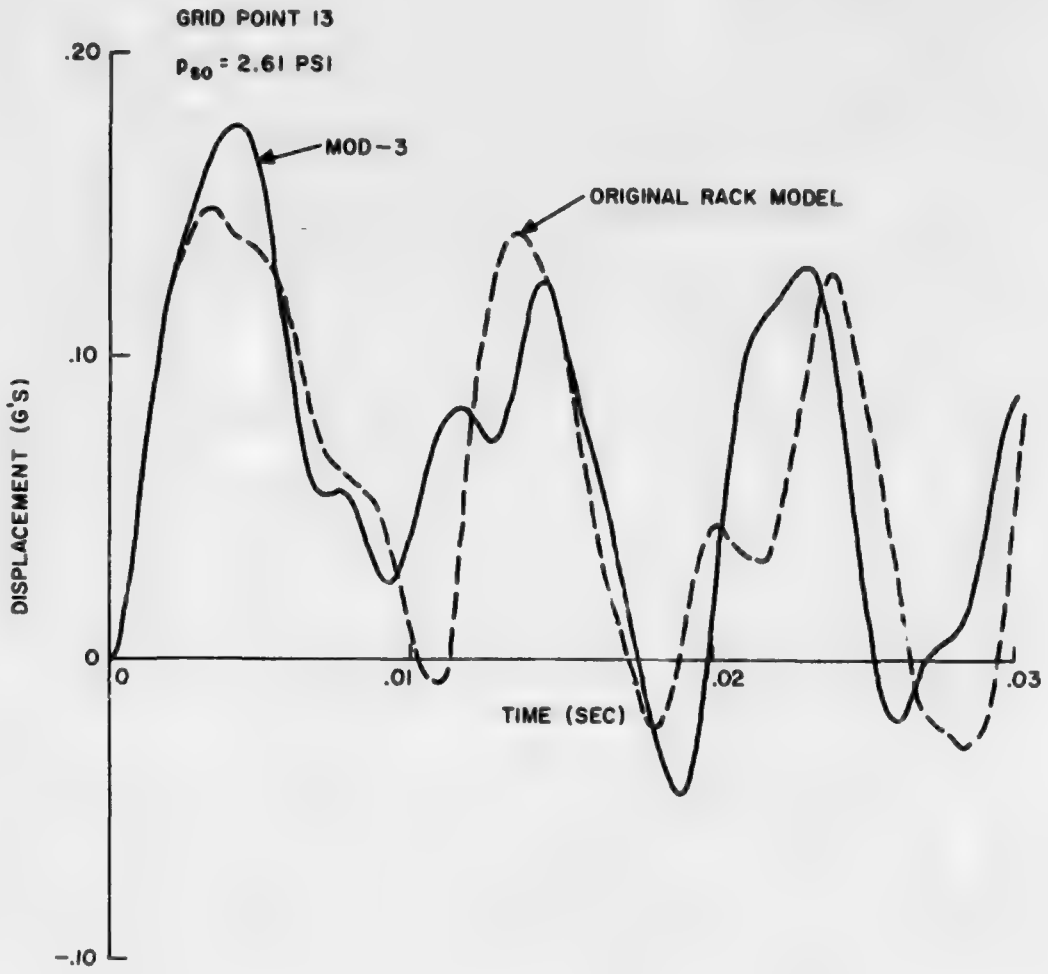

Figure 3.10. Comparison of Front Wall Displacements, Stage 2

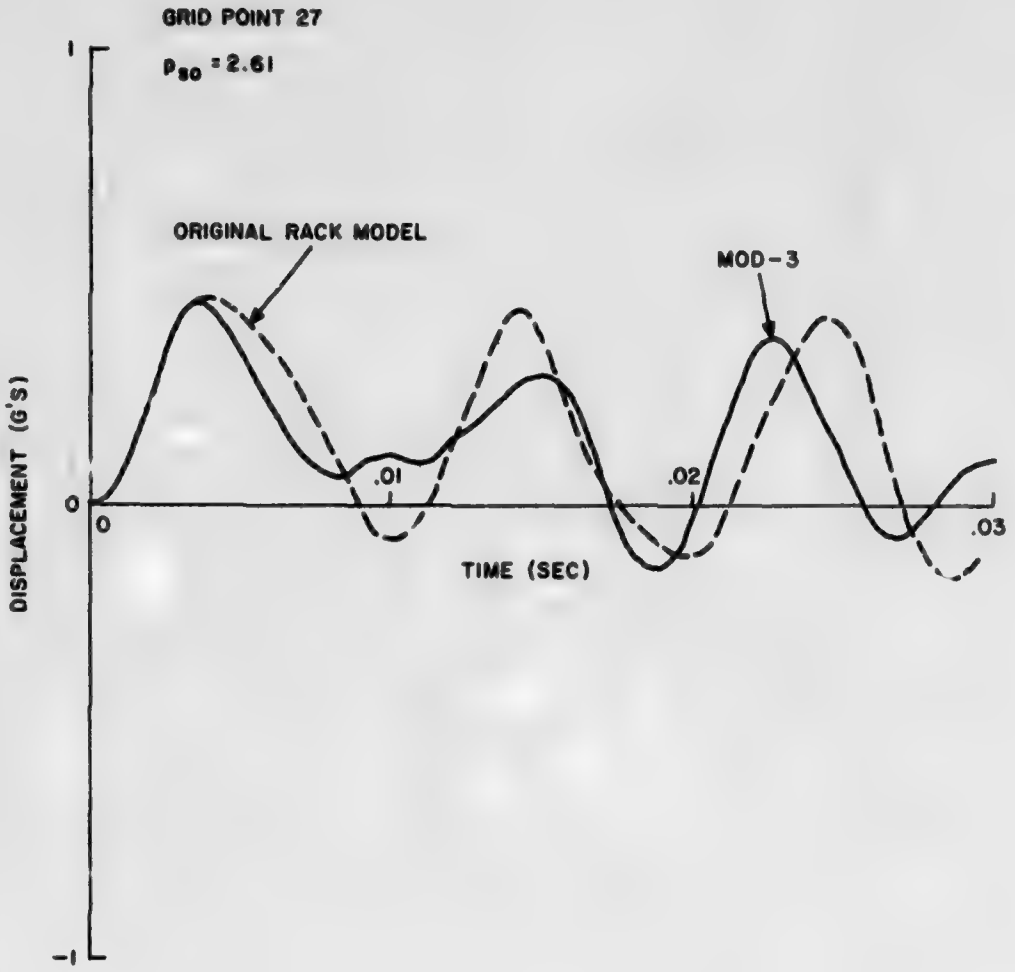

Figure 3.11. Comparison of Front Wall Displacements, Stage 2

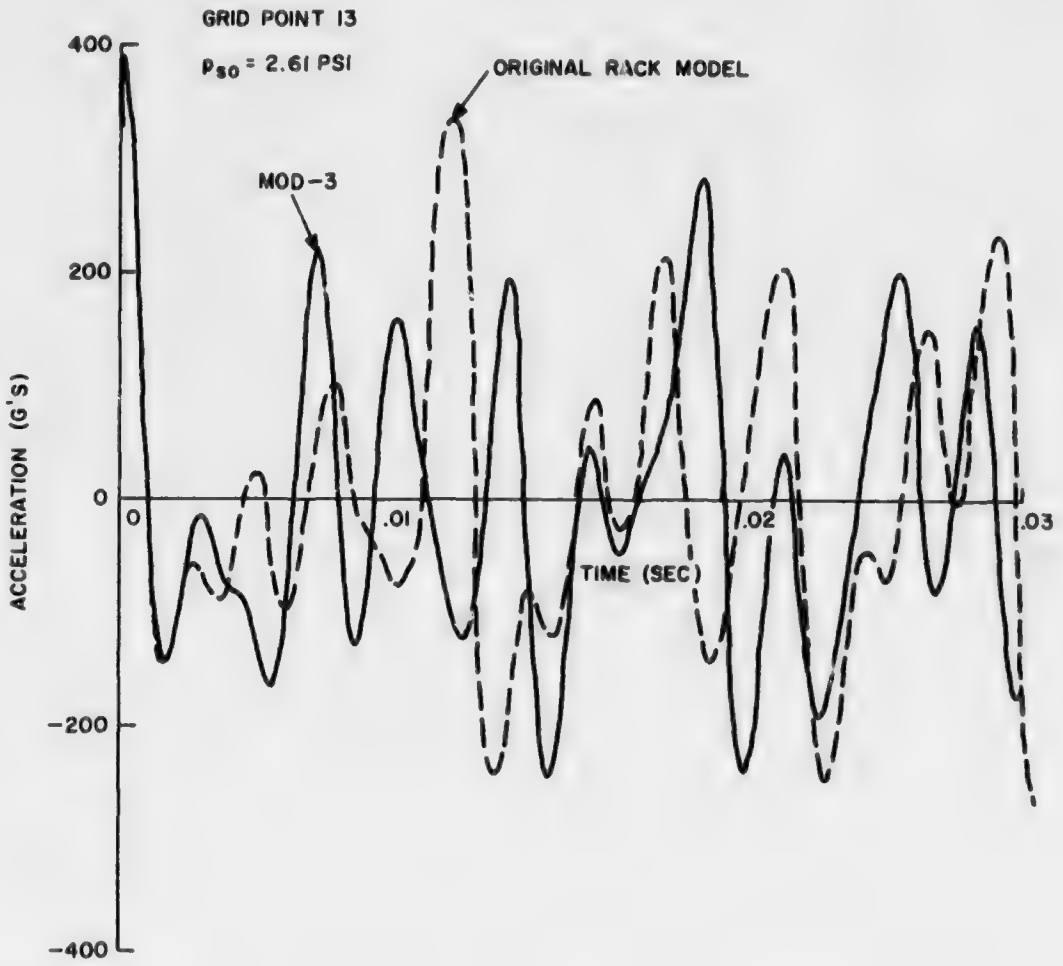

Figure 3.12. Comparison of Front Wall Accelerations, Stage 2

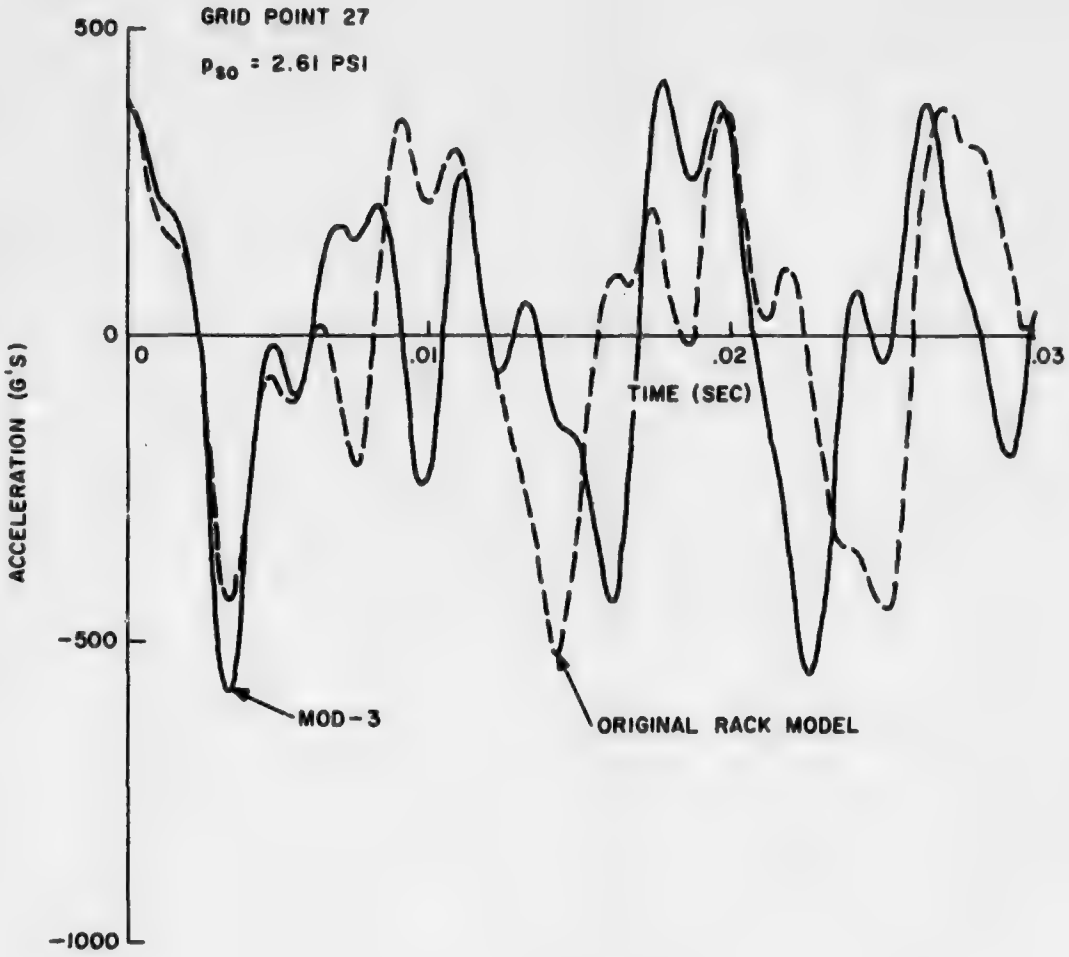

Figure 3.13. Comparison of Front Wall Accelerations, Stage 2

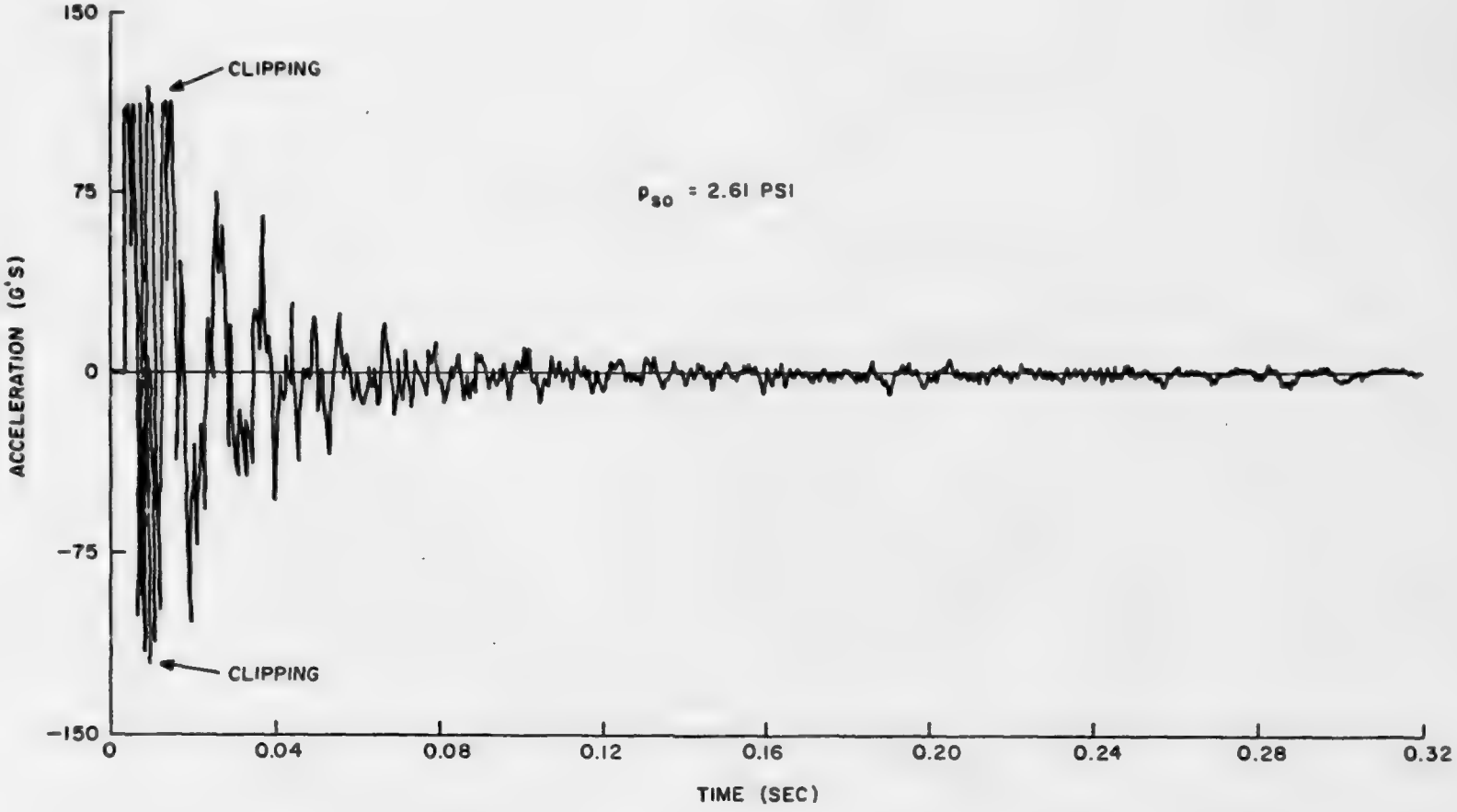

Figure 3.14. Front Wall Acceleration Measured at Station 3-7-A (Grid Point 13)

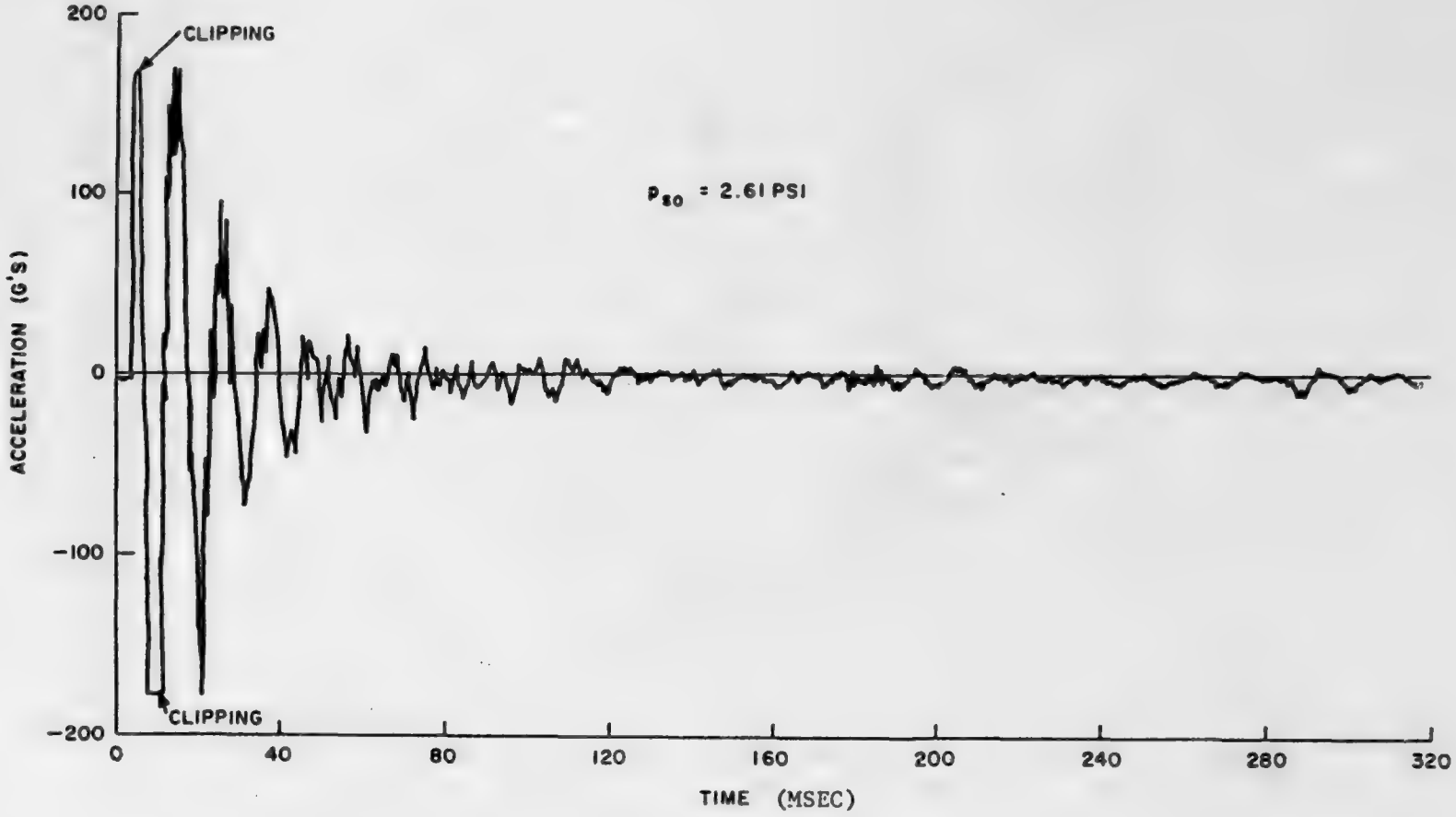

Figure 3.15. Front Wall Acceleration Measured at Station 3-4-A (Grid Point 27)

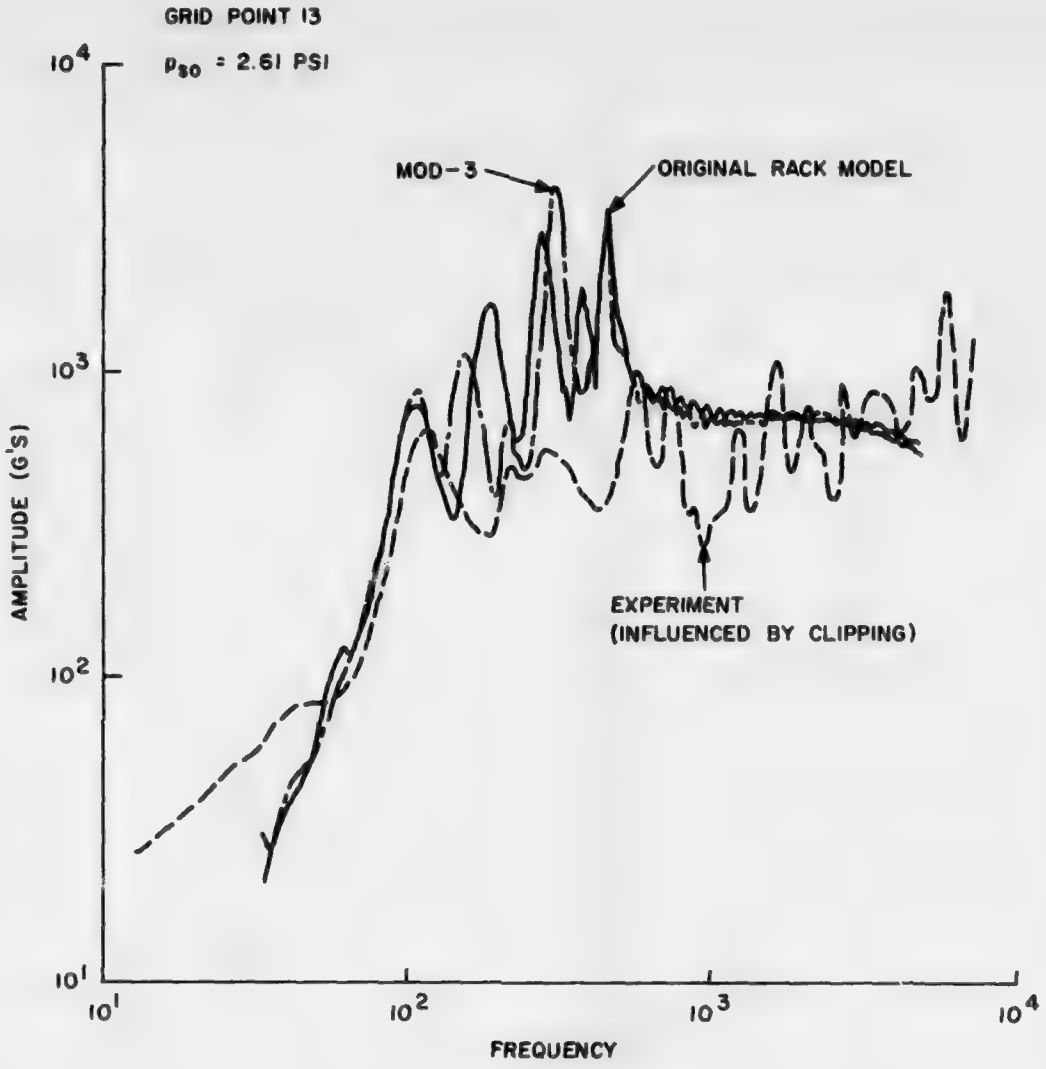

Figure 3.16. Comparison of Shock Spectra Based on Experimental and Analytical Acceleration Time Histories, (Front Wall), Stage 2

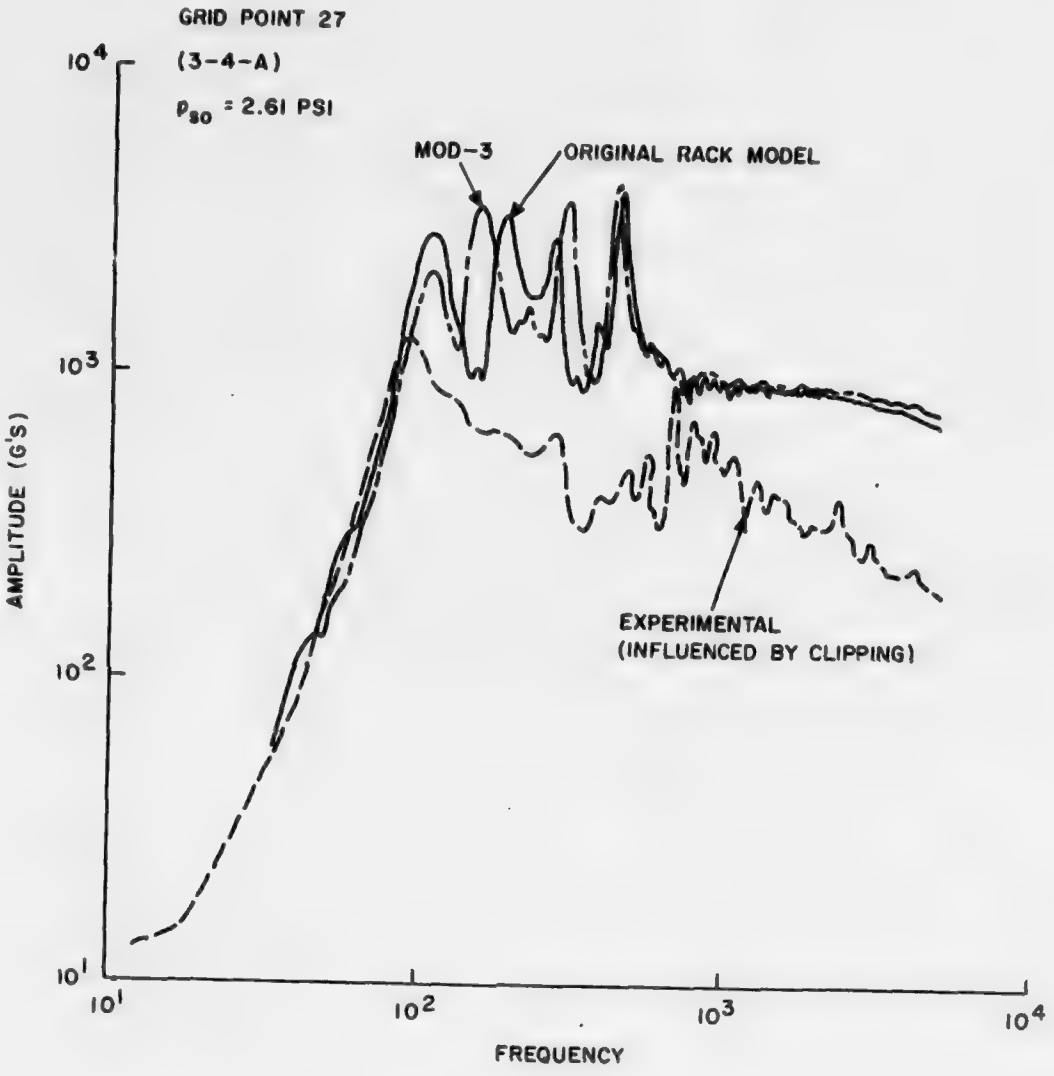

Figure 3.17. Comparison of Shock Spectra Based on Experimental and Analytical Acceleration Time Histories (Front Wall), Stage 2

The rack displacement response is compared in Fig. 3.18 for the modified and original rack models at grid point 92. Significant differences exist in the peak displacement, with the original model resulting in a substantially larger amplitude. The most noticeable effect of the rack wall modificatons, however, occurred in the rack accelerations, which are shown in Fig. 3.19 for each MOD. Comparing these responses with the rack accelerations based on the original rack model (Fig. 3.20), it is noted that the rack modifications resulted in a substantial increase in the rack acceleration from 20 g's to 50 g's. The modeling changes also introduced very high acceleration frequencies in each MOD case, frequencies which were originally "filtered" out by the less detailed structural definition of the original rack model.

Figure 3.21 shows the experimental acceleration time history of the rack at grid point 92. Comparing this with the analytical acceleration based on the original rack model (Fig. 3.20) it is evident that a disparity exists with regard to amplitude and frequency content. For example, the peak experimental amplitude is about 125 g's compared to 20 g's for the analytical case. The rack MODS offer an improvement in the acceleration time history amplitudes, by increasing the analytical level from 20 g's to 50 g's. This incidentally agrees with the 50 g's level occurring during the first four milliseconds of the experimental response in Fig. 3.21. However, the frequency content during this early time as well as in the remaining time period compares poorly for the experimental and analytical cases. The analytical response has a substantially higher frequency content (several thousand cps) whereas the experimental response lacks significant frequencies above approximately 500 cps. The presence of the higher analytical frequencies is attributed to the greater structural detail introduced into the rack model, and the lack of frequencies higher than 500 cps in the experimental response is probably attributed to the accelerometer gage which had a natural frequency of only 1250 cps.

Shock spectra comparisons are shown in Figs. 3.22-3.25 between the experimental case, based on the time history in Fig. 3.21, and for the analytical cases, based on the time histories of the original rack model and for MODS 1, 2 and 3. The disparity noted earlier between the test data and the original rack model is also reflected in the shock spectra in Fig. 3.22, which shows that the experimental spectrum is significantly larger over the entire frequency range. The rack modifications resulted in increasing the analytical shock spectra in Figs. 3.23-3.25, and at frequencies above 2000 cps the spectra overlap. Since the experimental data is lacking in frequencies much above 500 cps, a comparison of spectra at frequencies between 500 cps and 2000 cps is not meaningful and a basis does not exist for establishing a level of confidence in either the analytical responses or the test data in this frequency range.

In the lower frequency range (less than 1000 cps), it is also difficult to assign a level of confidence to the comparisons between theory and experiment since substantial differences still remain in the shock spectra and time history responses. A higher level of confidence does exist, though, compared to the higher frequency range, for the analytical responses and the experimental data. With regard

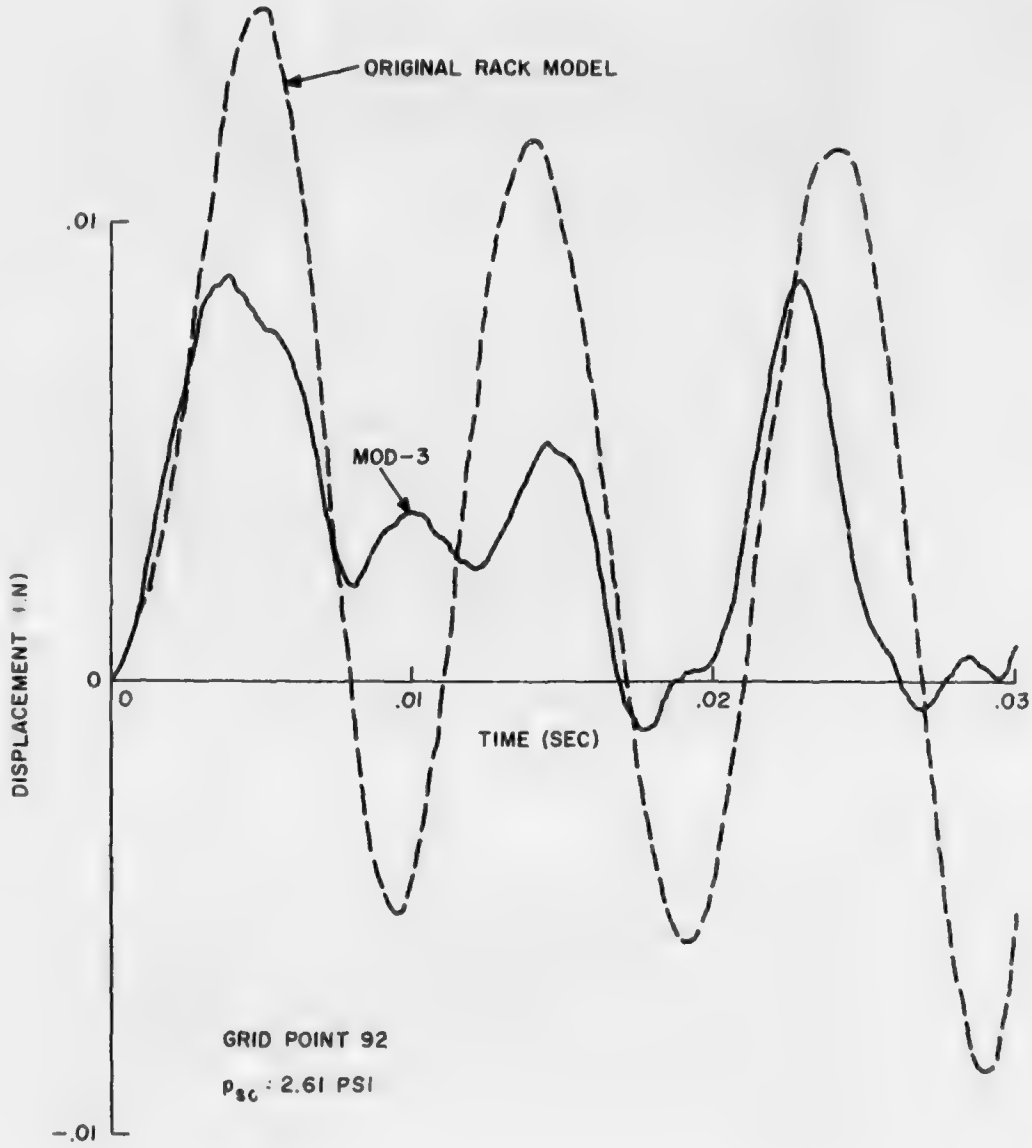

Figure 3.18. Comparison of Front Rack Displacements, Stage 2

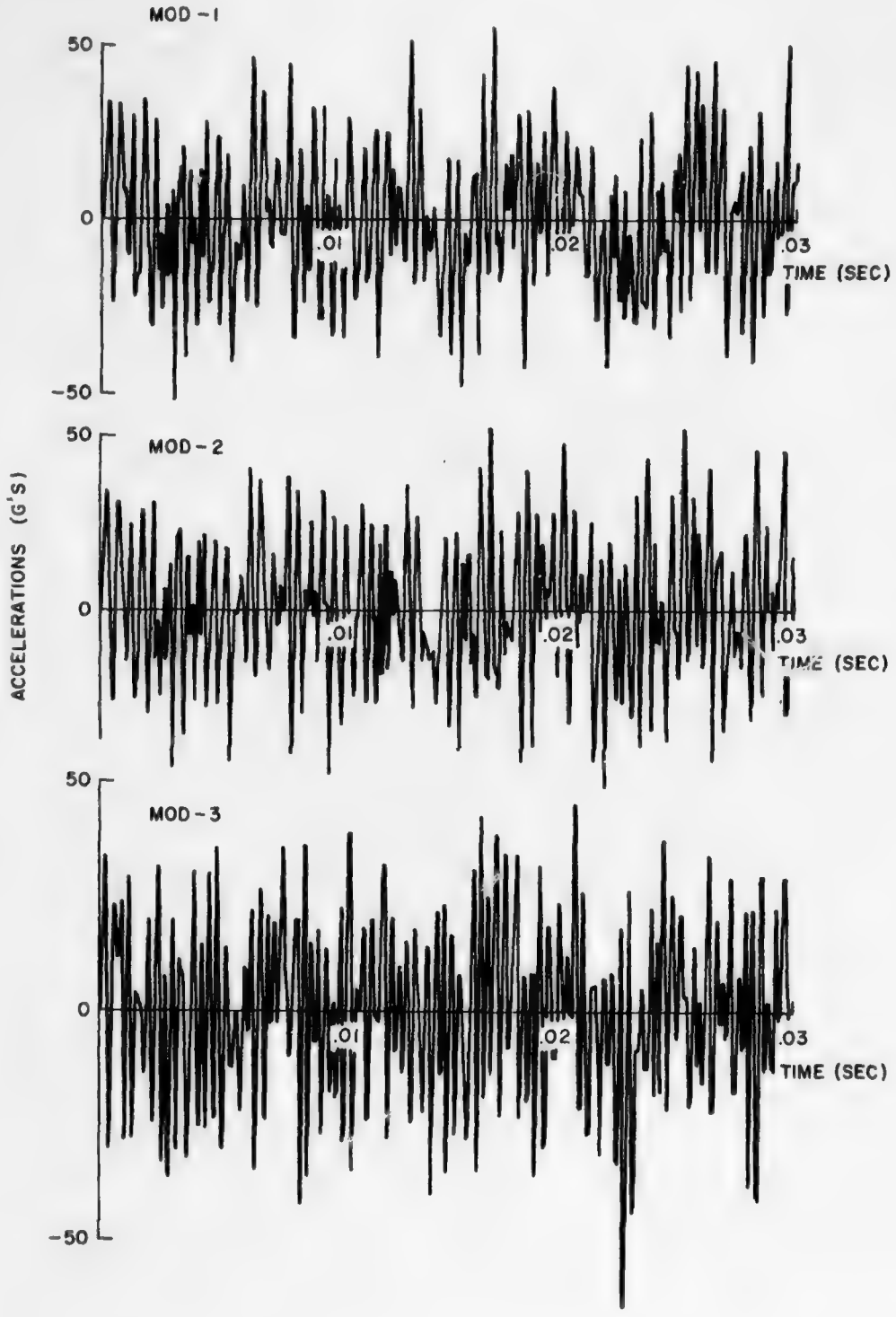

Figure 3.19. Front Rack Accelerations at Grid Point 92 for MOD-1, MOD-2 and MOD-3

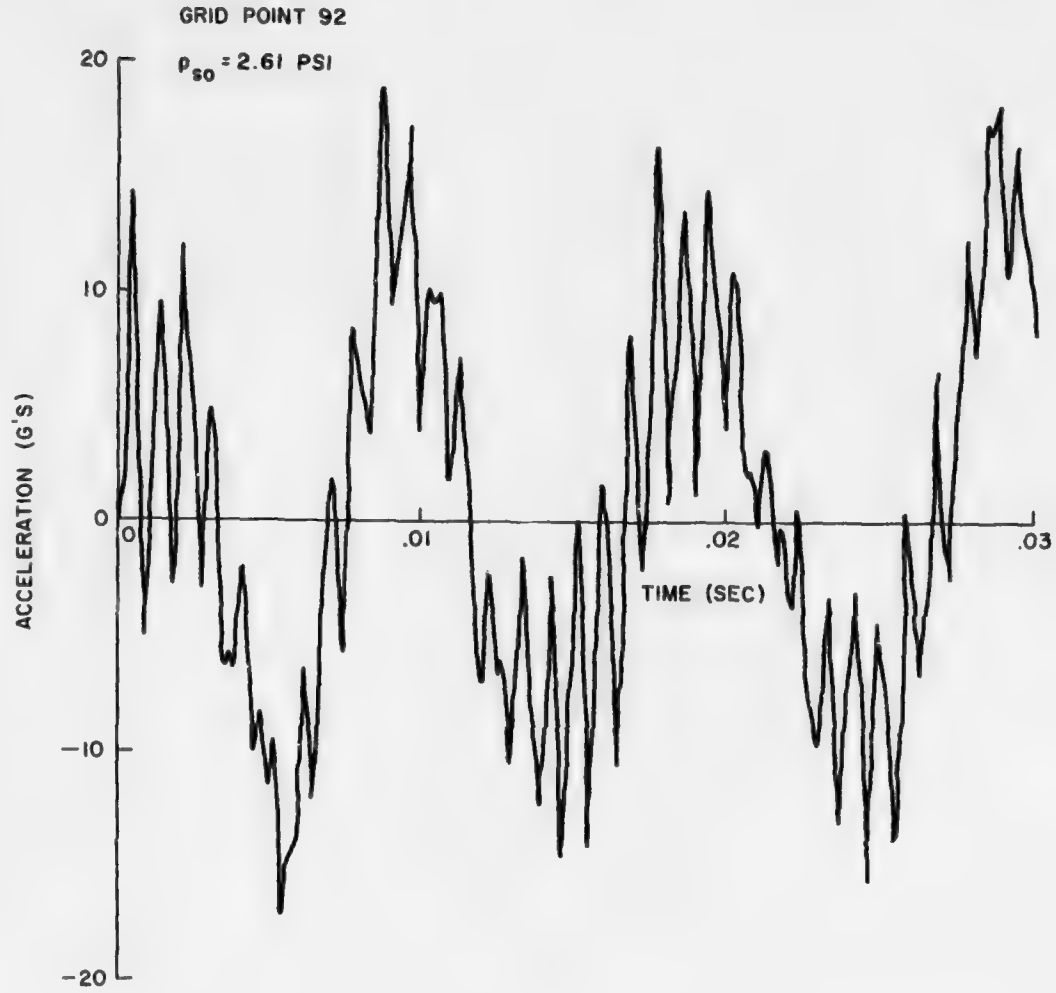

Figure 3.20. Front Rack Acceleration, Stage 2, Set 3, Original Rack Model

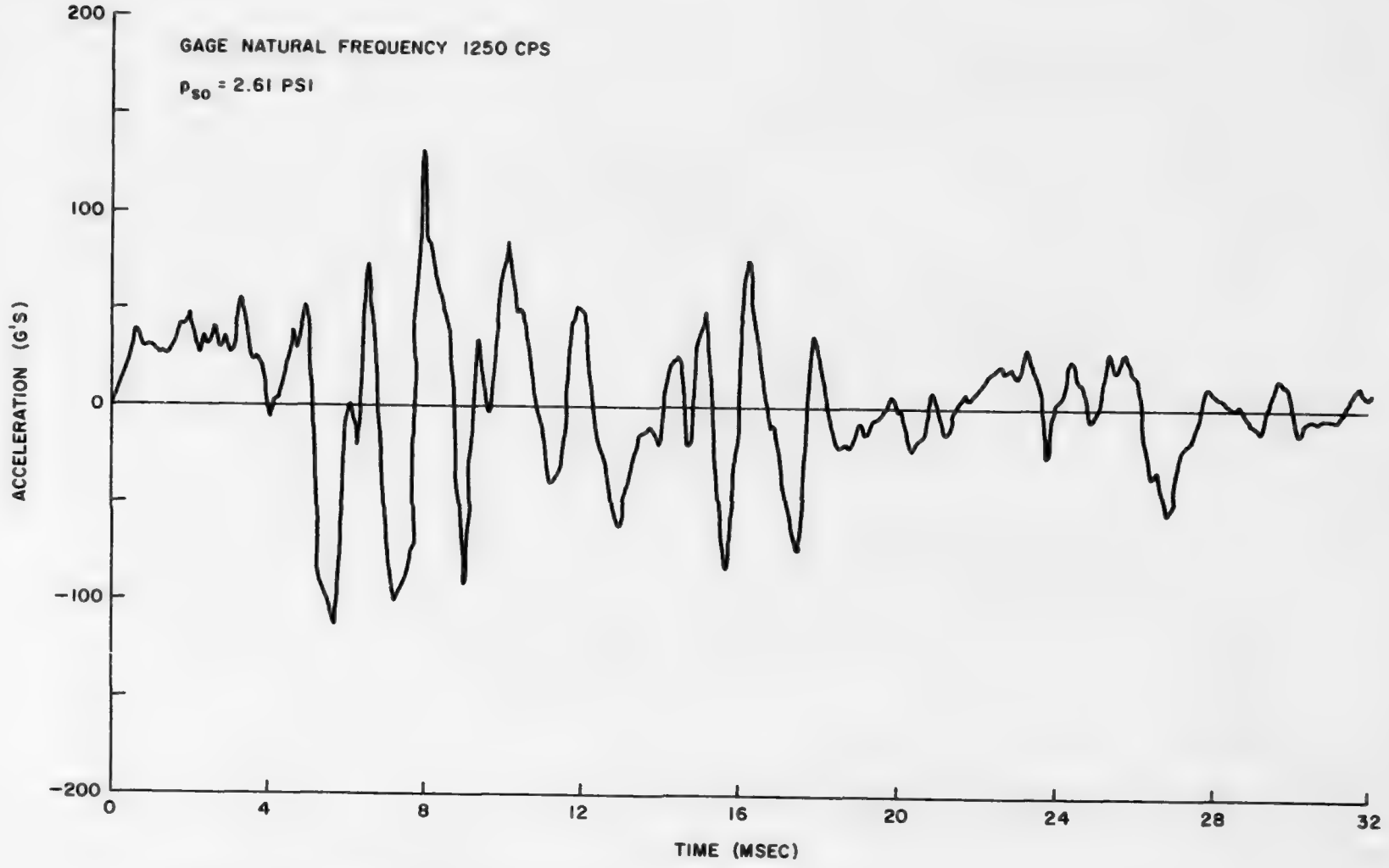

Figure 3.21. Front Rack Acceleration Measured at Station 3-4-AE (Grid Point 92)

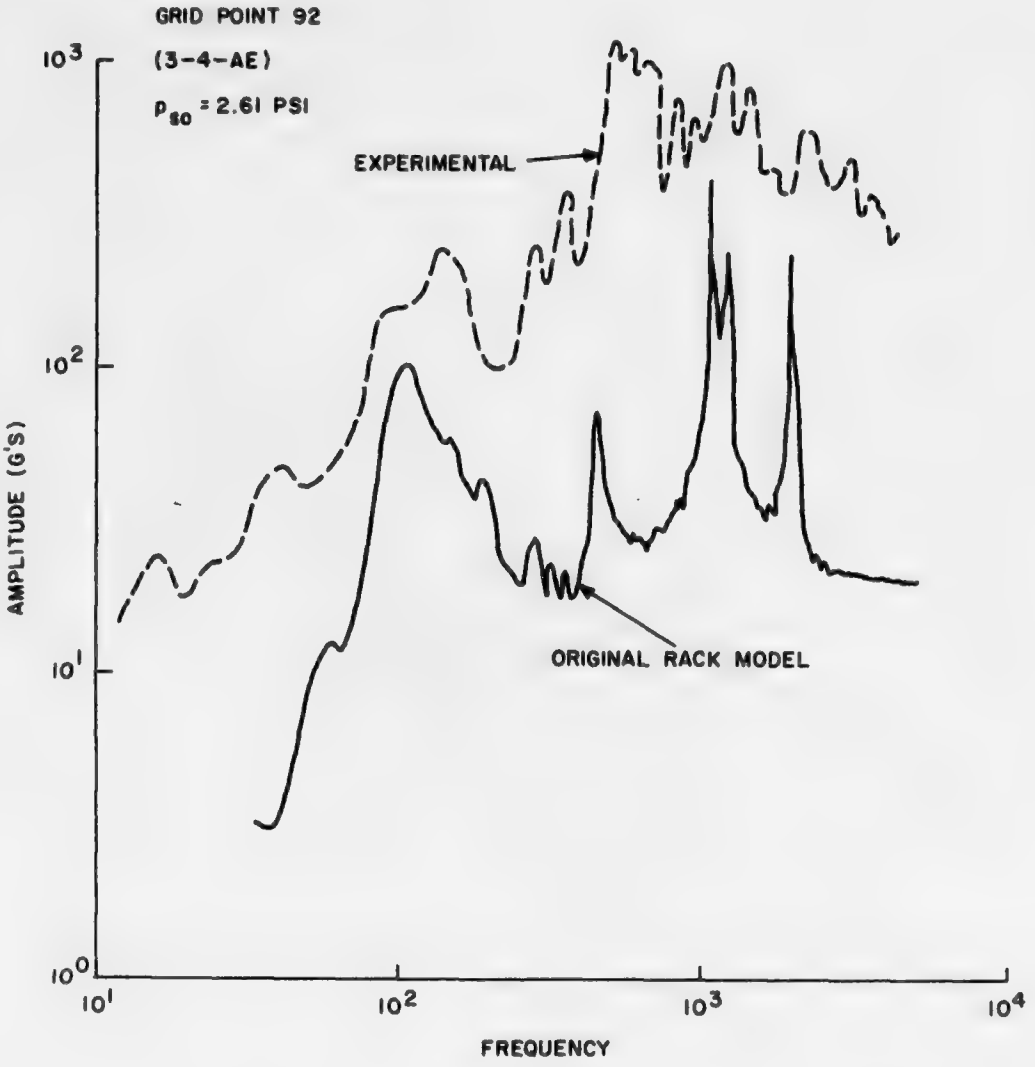

Figure 3.22. Comparison of Shock Spectra Based on Experimental and Analytical Acceleration Time Histories, (Front Rack), Stage 2

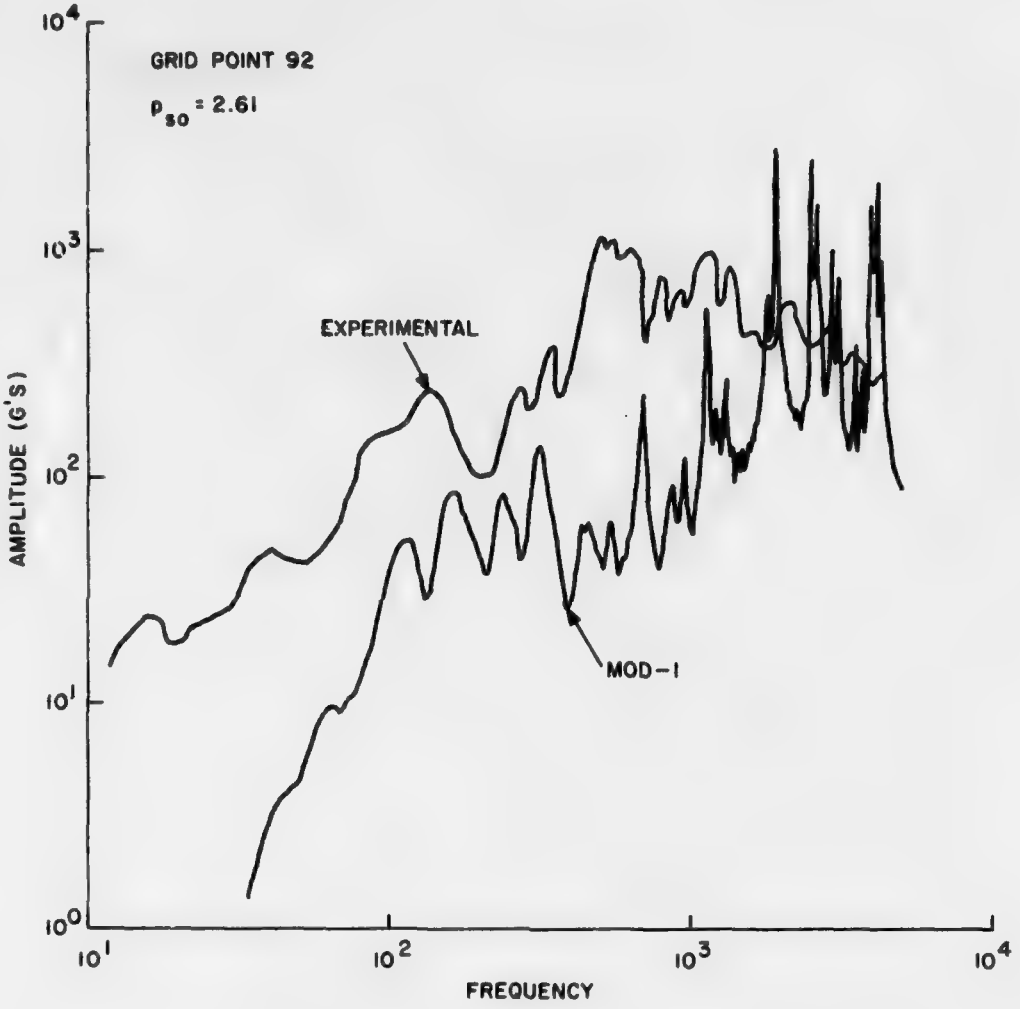

Figure 3.23. Comparison of Front Rack Shock Spectra

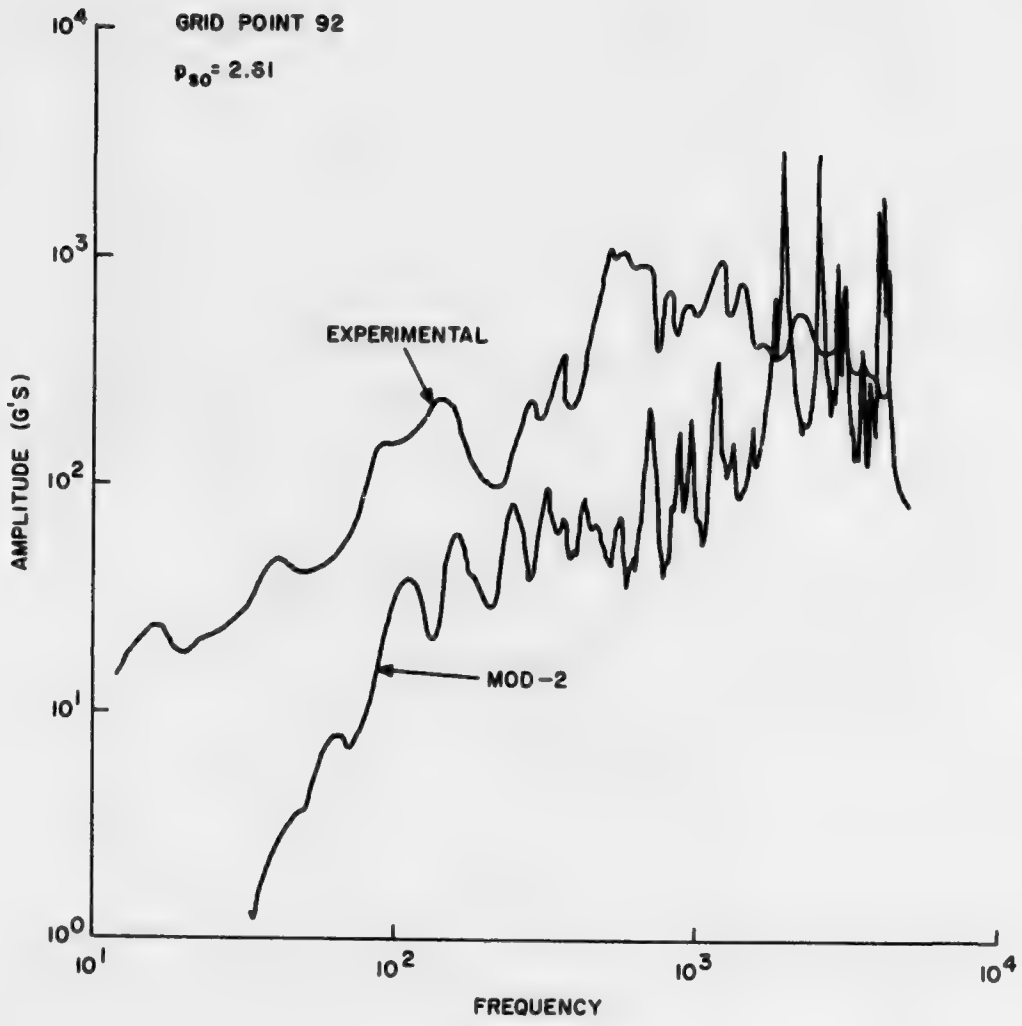

Figure 3.24. Comparison of Front Rack Shock Spectra

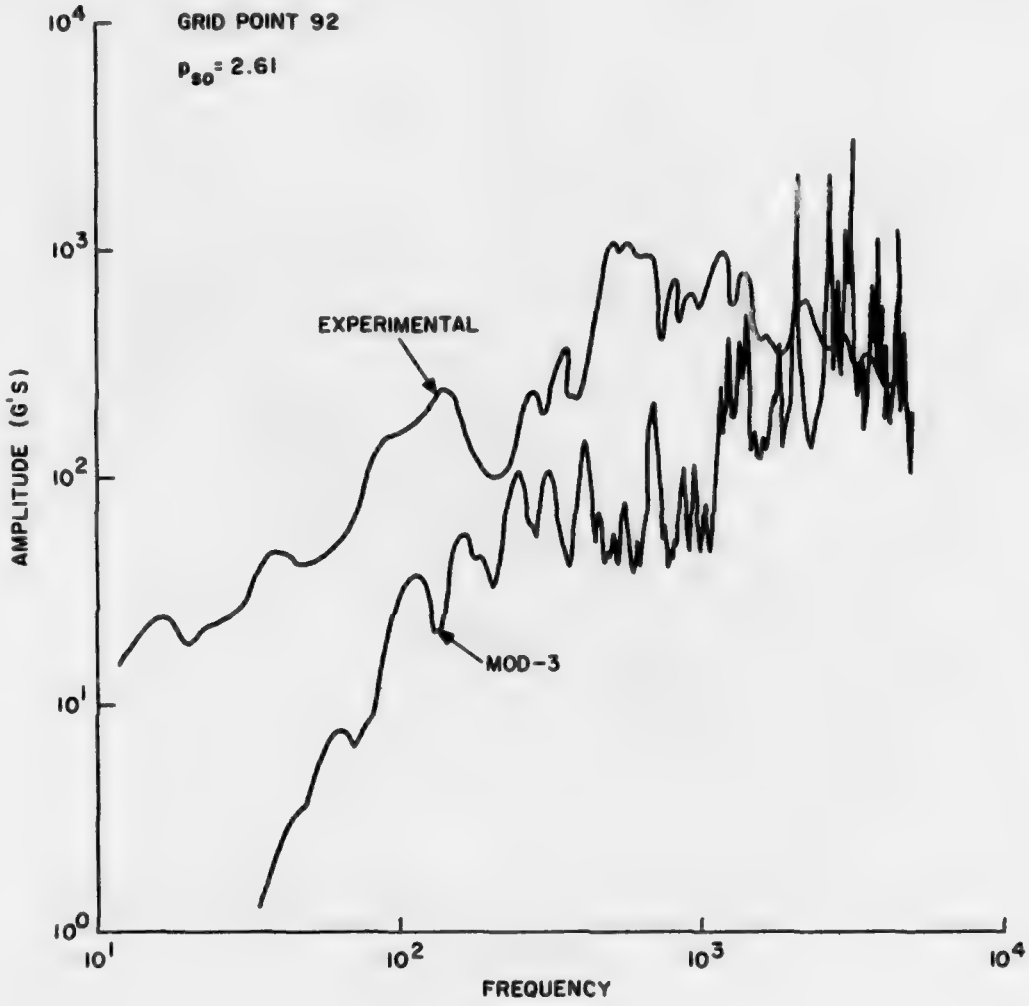

Figure 3.25. Comparison of Front Rack Shock Spectra

to the analytical model, it is generally recognized that the lower modes of a structure are usually more accurately represented than the higher modes (and more so for displacements than accelerations) because of inherent errors which are always present in a discretization of a continuous system. Since the responses of the least detailed (discretized) model, MOD-1, were very similar to the responses of the most detailed model, MOD-3, it is felt that within the existing constraints imposed on the modeling that a sufficiently detailed structural model was developed. This provides a reasonable level of confidence in at least the lower modes (frequencies) of the structure, though it does not provide an upper (confidence) bound on the frequency. With regard to the experimental data, a greater confidence level also exists in the lower frequency range, provided the frequencies are sufficiently less than the 1250 cps natural frequency of the gage.

On the basis of the available experimental and analytical data, it is thus felt that the true level of confidence in the correlation of the rack responses presented herein cannot be assigned. It appears reasonable that the confidence level is higher at frequencies less than 1000 cps, and more so for deflections than for accelerations. With regard to the wall responses, they were more consistent with the test data than were the rack responses. However, the clipped front wall test data also makes it difficult to establish a level of confidence in their predictions. It may be stated, though, that a higher confidence level exists in the wall responses than in the rack responses and that a cutoff frequency of approximately 1000 cps would also be reasonable at the present time as for the rack responses.

3.4 Summary

Improving the rack model introduced the higher harmonics which were "filtered" out by the original less detailed rack model. These higher modes resulted in a substantial increase in the rack accelerations but had little influence on the front wall responses. The increase in the rack response provided closer agreement with the experimental peaks during the first 4 msecs of response. At later times, however, a considerable difference still exists between the analytical and experimental results. At frequencies between 100 cps and 1000 cps, the shock spectra comparison improved, though the experimental spectrum is still considerably higher than the analytical spectrum. At higher frequencies the shock spectra overlap but a comparison here is not meaningful since the experimental rack data lacked significant frequencies beyond 500 cps. With regard to both the rack responses and the front wall responses, a higher level of confidence exists in their prediction at frequencies less than approximately 1000 cps than at higher frequencies. At the present time, though, the extent of the confidence level cannot be assigned, but it would be higher for the front wall responses than for the rack responses.

Comparing the results of one rack model versus another, the more detailed model, MOD-3, offered no substantial improvement over MOD-1. The most significant changes in response occurred when progressing from the original rack model to MOD-1, and this affected primarily the rack

response of interest. Therefore, the first rack modification, even though it neglects the stiffening effect of the equipment shelves, is an adequate representation and a more detailed model is unnecessary for computational purposes.

In spite of the improvement in the response resulting from improvements in the rack model, correlation of the rack response with the test data is still poor. The front wall acceleration comparison with test data is far more favorable, as indicated also in Ref. 1, though some complications are introduced since the test data was clipped due to gage saturation. It remains that the analytical and experimental front wall acceleration levels were generally of the same level, whereas the experimental rack accelerations exceeded the analytical levels substantially. It would appear that the experimental rack accelerations should be considerably lower than the wall acceleration because of the very substantial rack mass compared to the front wall mass. For example, the front wall weighs approximately 160 lbs and the weighted front racks weigh 2000 lbs total. The measured front wall and rack accelerations are of the same order whereas the analytical front wall acceleration exceeds the rack acceleration by about a factor of ten, which is consistent with the weight ratio.

With regard to the quality of the experimental data, an accelerometer with a natural frequency in the frequency range of the measurement being made was used. Also, the accelerometer was mounted on a rack surface whose response could contaminate the desired measurement. These factors could introduce serious errors in the experimental results. Another consideration is the possible influence of the rigid body shelter response in the test measurements.

Analytical uncertainties still remain in the modeling. The rack model modifications considered herein included a better load path within the rack structure and more detailed structural definitions of the rack geometry than for the original rack model. These modifications were made using the original boundary conditions, load transfer mechanism from the shelter wall to the rack structure, types of connectivity between the structural elements, and omitted shelter rigid body motions. It was not the purpose of this present report to also investigate changes in these factors, however they can have a significant influence on the response. For example, the experimental data in Fig. 3.21 shows that the character of the response during the first four milliseconds is inconsistent with the character of the response during the remaining time period, a possible indication of the influence of some rigid body motion of the shelter which was not accounted for in the modeling.

SECTION 4
MAJOR CONCLUSIONS

This report had two primary objectives in the current NASTRAN finite element analysis of the blast response of electronic equipment shelters and internally mounted equipment. The first involved the response of the complete shelter-rack system, investigating the effects of tie-down cables, and comparing with the responses obtained with a simpler structural model. The second objective was to refine the original rack model of Ref. 1 for the purpose of improving the comparisons of the rack accelerations with test data. Three rack model modifications were developed. MOD-1 had a finer grid mesh, more structural elements and improved load paths than the original rack model, MOD-2 was an extension of MOD-1 to include the stiffening effects of the equipment shelves and MOD-3 was an extension of MOD-2, incorporating additional structural elements. In each case, the responses were obtained for a shock wave of 2.61 psi incident overpressure impinging on the front wall of the shelter.

The major results of the study are:

1. The accelerations and displacements on the front wall and front rack obtained with the complete shelter model were similar to those obtained with the simpler model. This is attributed primarily to the dominant weight-stiffness combination provided by the steel weighted racks in proportion to the remaining shelter structure.

2. The effect of the tie-down cables on the complete shelter response was negligible except locally at the cable attachment points.

3. The results obtained by rack MODS 1, 2 and 3 were quite similar, therefore no benefit was derived by the more detailed MOD-3. The most significant changes in response occurred when progressing from the original rack model to MOD-1.

4. The stiffening effects of the rack shelves were minor (MOD-2 vs MOD-1), and the shelf mass appears to be the primary structural shelf item (for the present rack system).

5. Rigid body motion of the shelter may be present in the measured accelerations. This was not modeled in NASTRAN since the ground resistance forces were not known (also, the skids were buried). In NASTRAN, the shelter and racks were clamped at the base.

6. The front wall accelerations and shock spectra were more consistent with the experimental data than were the rack responses.

7. Refinements in the rack model introduced higher harmonics which were "filtered" out by the original less detailed model of Ref. 1.

8. The higher harmonics introduced by the more detailed rack models resulted in a substantial increase in the rack accelerations and improved the comparison in amplitude with the measured rack response. The shock spectrum was also improved at frequencies between 100 and 1000 cps, but was still lower than the experimental shock spectrum in this frequency range. At frequencies above 1000 cps, the analytical shock spectrum exceeded the experimental shock spectrum because of the higher frequencies introduced by the rack modifications.

9. In spite of the increase in the rack accelerations and the corresponding shock spectra resulting from the rack model refinements, the correlation with the rack test data is still considered poor. It is believed, though, that a higher confidence level exists in the analytical and experimental results at frequencies less than 1000 cps than at the higher frequencies. This confidence level is greater for the front wall responses than for the rack responses.

The racks considered here were hardmounted to the shelter structure and therefore provided additional strengthening and stiffening to the shelter. This arrangement, however, provided no mechanism for shock isolation of equipment which may be mounted on the rack shelves. With proper isolation, the rack accelerations would be lower than the levels experienced in this report. Another report in the current effort, Ref. 2, presents a modeling study of a monolithic rack system mounted on wire rope coil isolators in an S-280 shelter under blast loading.

Ref. 2. Calligeros, John M., Finite Element Analysis of the Blast Response of a Complete Shelter with Isolator-Mounted Equipment Racks, KA TR-123, July 1975.

APPENDIX A

TIE-DOWN GUY CABLE MODELING

Each of the upper and lower corners of the shelter in the DIAL PACK test was secured to an anchor point in the ground by a 3/8 inch diameter steel guy cable. Modeling of the lower guy cables was unnecessary since the base of the shelter was assumed clamped. Figure A.1 presents a schematic of the tie down cable configuration for grid point 43 which is located at an upper shelter corner on the windward side. A similar configuration exists for the cable connected to grid point 102 on the leeward side.

The cables connected to the upper shelter corners were pretensioned before blast loading by rotating a turnbuckle. Denoting the tensile preload as F_0, the components of force applied by F_0 to grid point 43 are

$$\begin{aligned} F_{01} &= -F_0 \frac{a}{L} \\ F_{02} &= -F_0 \frac{d}{L} \\ F_{03} &= -F_0 \frac{c}{L} \end{aligned} \qquad \text{(A.1)}$$

where the symbols and coordinate system are defined in Fig. A.1. The application of the preload by the turnbuckle rotation translates grid point 43 to point A whose coordinates are u_{01}, u_{02}, u_{03}. During blast loading, a stretch ε (from A to B) in the cable results which, for small displacements, may be expressed as

$$\varepsilon = \frac{a}{L}(u_1-u_{01}) + \frac{d}{L}(u_2-u_{02}) + \frac{c}{L}(u_3-u_{03}) \qquad \text{(A.2)}$$

where u_1, u_2, u_3 are the coordinates of grid point 43 at any time after blast disturbance (point B). The displacements u_{01} and u_1 are measured from a local frame whose origin is the original location of grid point 43, i.e., the location of grid point 43 before the application of the preload F_0 (see Fig. A.1). The stretch ε is thus the additional stretch in the cable when the cable end is displaced from its static preloaded location. The cable force resulting from the stretch ε is

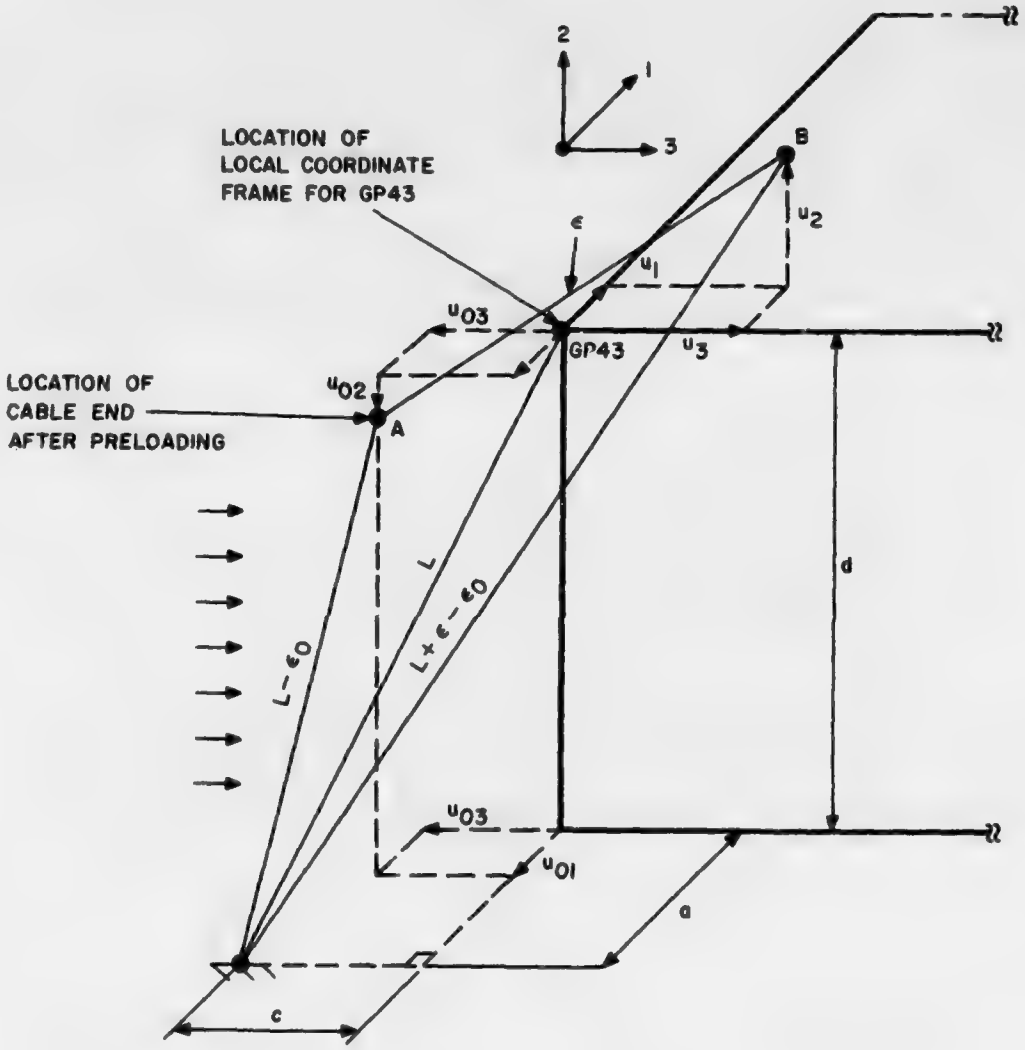

Figure A.1 - Guy Cable Terminology

$$F_\varepsilon = \frac{AE}{L}\,\varepsilon \tag{A.3}$$

which results in the following force components applied to grid point 43

$$\begin{aligned} F_{\varepsilon 1} &= -\left(\frac{AE}{L}\,\varepsilon\right)\,\frac{a}{L} \\ F_{\varepsilon 2} &= -\left(\frac{AE}{L}\,\varepsilon\right)\,\frac{d}{L} \\ F_{\varepsilon 3} &= -\left(\frac{AE}{L}\,\varepsilon\right)\,\frac{c}{L} \end{aligned} \tag{A.4}$$

Substituting Eq. (A.2) into Equation (A.4) and summing with Eqs. (A.1), the total force components F_1, F_2, F_3 applied to grid point 43, by the cable, which include the effect of the preload, are

$$\begin{aligned} F_1 &= K_1 T \\ F_2 &= K_2 T \\ F_3 &= K_3 T \end{aligned} \tag{A.5}$$

where

$$T = -\left(\frac{F_0 L}{AE} + \varepsilon_0\right) - \varepsilon_1$$

$$\varepsilon_0 = -\frac{a}{L}\,u_{01} + \frac{d}{L}\,u_{02} + \frac{c}{L}\,u_{03} \tag{A.6}$$

$$\varepsilon_1 = \frac{a}{L}\,u_1 + \frac{d}{L}\,u_2 + \frac{c}{L}\,u_3$$

and

$$\begin{aligned} K_1 &= \frac{AE}{L^2}\,a \\ K_2 &= \frac{AE}{L^2}\,d \\ K_3 &= \frac{AE}{L^2}\,c \end{aligned} \tag{A.7}$$

$|T|$ represents the total stretch in the cable measured from its position before the preload F_0 is applied. The slackened state of the cable at any time is attained when T=0, i.e., when

$$\varepsilon_1 = -\left(\frac{F_0 L}{AE} + \varepsilon_0\right) \tag{A.8}$$

A similar procedure yields the following cable force components which are applied to grid point 102 at the upper shelter corner on the leeward side

$$\begin{aligned} F_1 &= K_1 T \\ F_2 &= K_2 T \\ F_3 &= -K_3 T \end{aligned} \tag{A.9}$$

where T and K_1, K_2, K_3 are given by Eqs. (A.6) and (A.7), respectively. The expressions for ε_0 and ε_1 become

$$\begin{aligned} \varepsilon_0 &= -\left(\frac{a}{L} u_{01} + \frac{d}{L} u_{02} - \frac{c}{L} u_{03}\right) \\ \varepsilon_1 &= \frac{a}{L} u_1 + \frac{d}{L} u_2 - \frac{c}{L} u_3 \end{aligned} \tag{A.10}$$

Figure A.2 presents a summary of the cable force components for grid point 43 and grid point 102.

An "extra point" (EPOINT) was established in NASTRAN to represent ε_1 and the function T was tabulated on a TABLED1 card for given values of F_0, u_{01}, u_{02}, u_{03} with ε_1 as the independent variable. Each force component F_1, F_2, F_3 was modeled by a NOLIN1 card which referenced the EPOINT ε_1.

The cable parameters are

$$\begin{aligned} A &= 0.1104 \text{ in}^2 \\ E &= 29 \times 10^6 \text{ lb/in}^2 \\ L &= 123.04 \text{ in} \end{aligned} \tag{A.11}$$

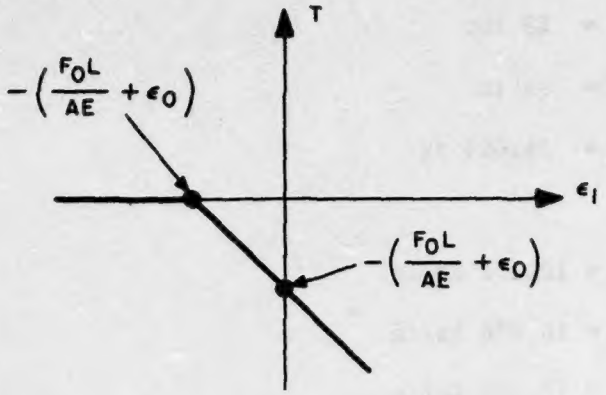

$$T = -\left(\frac{F_0 L}{AE} + \epsilon_0\right) - \epsilon_1$$

Grid Point 43	Grid Point 102
$\epsilon_0 = -\left(\frac{a}{L} u_{01} + \frac{d}{L} u_{02} + \frac{c}{L} u_{03}\right)$	$\epsilon_0 = -\left(\frac{a}{L} u_{01} + \frac{d}{L} u_{02} - \frac{c}{L} u_{03}\right)$
$\epsilon_1 = \frac{a}{L} u_1 + \frac{d}{L} u_2 + \frac{c}{L} u_3$	$\epsilon_1 = \frac{a}{L} u_1 + \frac{d}{L} u_2 - \frac{c}{L} u_3$
$F_1 = K_1 T$ $F_2 = K_2 T$ $F_3 = K_3 T$ } Cable Force Components	$F_1 = K_1 T$ $F_2 = K_2 T$ $F_3 = -K_3 T$ } Cable Force Components

Figure A.2. Cable Force Representation

$$a = 48 \text{ in.}$$

$$c = 84 \text{ in.}$$

$$d = 76.024 \text{ in.}$$

and

$$K_1 = 10{,}151 \text{ lb/in}$$

$$K_2 = 16{,}078 \text{ lb/in} \qquad \text{(A.12)}$$

$$K_3 = 17{,}765 \text{ lb/in}$$

The displacement components u_{01}, u_{02}, u_{03} at grid points 43 and 102 were obtained by the NASTRAN static solution rigid format for a preload F_0 = 2000 lbs in each of the tie-down cables. At grid point 43

$$u_{01} = -0.00107 \text{ in.}$$

$$u_{02} = -0.00209 \text{ in.} \qquad \text{(A.13)}$$

$$u_{03} = -0.00149 \text{ in.}$$

for which Equations (A.6) yield

$$\varepsilon_0 = 0.002726 \text{ in.} \qquad \text{(A.14)}$$

$$T = -0.07959 - \varepsilon_1$$

At grid point 102,

$$u_{01} = -0.001172 \text{ in.}$$

$$u_{02} = -0.002059 \text{ in.} \qquad \text{(A.15)}$$

$$u_{03} = 0.001477 \text{ in.}$$

for which Equation (A.10) yields

$$\varepsilon_0 = 0.002738 \text{ in.} \qquad \text{(A.16)}$$

$$T = -0.07960 - \varepsilon_1$$

LIST OF SYMBOLS

A	cross-sectional area (in^2)
a,b,c	guy cable geometry (defined in Figure A.1)
CBAR	NASTRAN beam element
E	modulus of elasticity (lb/in^2)
F_ε	cable force associated with stretch ε (lbs)
F_0	cable preload (lbs)
K_1, K_2, K_3	constants defined in Equation (A.7) (lb/in)
L	original length of guy cable (in)
p_{so}	peak incident overpressure (lb/in^2)
T	total stretch in cable measured from position before application of preload (in)
u_{01}, u_{02}, u_{03}	static displacement components of guy cable end due to preload (defined in Figure A.1) (in)
u_1, u_2, u_3	displacement components in directions 1,2,3, respectively (in)
ε	cable stretch from preload position (in)
ε_0	cable stretch associated with displacements u_{01}, u_{02}, u_{03} (defined in Equation (A.6) (in)
ε_1	cable stretch associated with displacements u_1, u_2, u_3 (defined in Equation (A.6)) (in)